

3-D Seismic Structural Interpretation: Insights to Thrust Faulting and Paleo-Stress Field Distribution in the Deep Offshore Orange Basin, South Africa.

A mini-thesis submitted in partial fulfilment of the requirement for the degree of Magister Scientia in the Department of Earth Science, University of the Western Cape



By

Brian Msizi Cindi

Supervisor: Dr M. Opuwari

Co-supervisor: Prof. J.M. van Bever Donker

September 2016

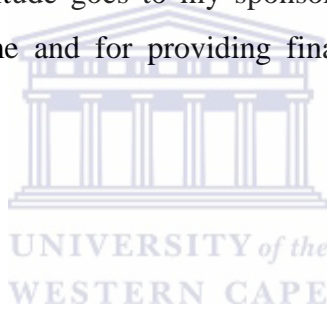
ACKNOWLEDGEMENT

The success of this thesis would not be possible if it was not for the assistance and support of my friends, family, my sponsor, mentors, writing coaches and the academic staff in the department of geology.

I would like to send my deep appreciation to my co-supervisor Prof Jan van Bever Donker for providing me with very insightful skills for the improvement and completion of this thesis. I would also like to thank my supervisor Dr M. Opuwari for giving me ideas and strategies on how to move forward.

I would also like to give my gratitude to the following persons who influenced me positively and who also assisted towards the completion of this project. These are Monica Oghenekome, Dominick Nehemiah, Chris Samakinde, Fritz Agbor, Pascal Awo Ojong, Dumisa Kevin January, Marc Ngama and Pricilla Lerato Ramphaka.

My deepest and sincere gratitude goes to my sponsor Shell Exploration & Production Company for believing in me and for providing financial and moral support when I needed it the most.



DECLARATION

I declare that “*3-D Seismic structural interpretation: Insights to thrust faulting and paleo-stress distribution in the deep offshore Orange Basin, South Africa:* ” is my own work, that it has not been submitted before for any degree or examination in any other university, and that all the sources used or quoted have been indicated and acknowledged as complete references.

Brian Msizi Cindi

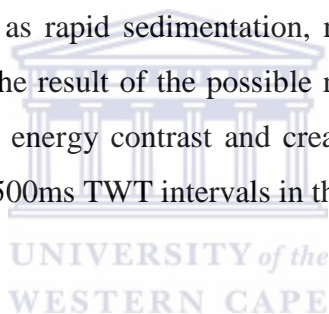
September 2016

Signed.....



ABSTRACT

The Orange Basin provides exceptional 3-D structures of folds and faults generated during soft-sediment slumping and deformation which is progressive in nature. 3-D seismic and structural evaluation techniques have been used to understand the geometric architecture of the gravity collapse structures. The location of the seismic surveyed area is approximately 370 km northwest of the Port of Saldanha. The interpretation of gravitational tectonics indicate significant amount of deformation that is not accounted for in the imaged thrust belt structure. The Study area covers 8200 square kilometre (km²) of the total 130 000 km² area of the Orange Basin offshore South Africa. The south parts of the Study area are largely featureless towards the shelf area. The north has chaotic seismic facies as the result of an increase in thrust faults in seismic facies 2. Episodic gravitational collapse system of the Orange Basin margin characterizes the late Cretaceous post-rift evolution. This Study area shows that implications of stress field and thrust faulting to the thickness change by gravity collapse systems are not only the result of geological processes such as rapid sedimentation, margin uplift and subsidence, but also could have occurred as the result of the possible meteorite impact. These processes caused gravitational potential energy contrast and created gravity collapse features that are observed between 3000-4500ms TWT intervals in the seismic data.



KEYWORDS:

Orange Basin, Tectonics, Gravity collapse systems, 3-D seismic data, Detachment, Stress field, Meteorite Impact

CONTENTS

ACKNOWLEDGEMENT	i
DECLARATION	ii
ABSTRACT.....	iii
KEYWORDS:.....	iii
CONTENTS.....	iv
LIST OF FIGURES	vi
CHAPTER 1	1
1. Introduction.....	1
1.2 Aims and Objective	2
1.3 Location of the Study area	2
1.4 Tectonic Setting of the Orange Basin	3
1.5 Basin Fill and Evolution	4
CHAPTER 2	6
2. Literature Review.....	6
2.1 Previous Studies.....	6
2.1.1 Regional Seismic Stratigraphy of the Orange Basin.....	6
2.1.1.1 Synrift Megasequence.....	6
2.1.1.2 Post rift Megasequence	7
2.1.2 Gravity-driven Systems of the Orange Basin.....	8
2.2.3 Comparison of the Orange Basin with other gravity collapse systems.....	10
2.2 Problem Statement.....	11
CHAPTER 3	12
3 Methodology	12
CHAPTER 4	14
4 Results.....	14
4.1 Seismic Analysis.....	14
4.1.1 Introduction.....	14
4.2 Horizon Interpretation.....	15
4.3 Thickness extraction	17
4.3.1 Introduction.....	17
4.3.2 Isochron Maps.....	17
4.4 Thrust faulting.....	22
4.5 Rose Diagrams Orientation.....	25
4.5.1 Introduction.....	25

4.5.2	Interpretation	25
4.6	Stereo-Net Plots Interpretation	26
4.6.1	Interpretation	26
CHAPTER 5	29
5.	Discussion	29
5.1	Development in deformation in the Study area	29
5.2	The stress and strain distribution in the Orange Basin	30
5.3	The Origins of the gravity collapse systems of the Orange Basin.....	31
5.3.1	Passive margin uplift and thermal subsidence.....	31
5.3.2	Meteorite impact in the Orange Basin.....	33
5.3.3	Slump sediment deformation.....	37
CHAPTER 6	40
6.1	Conclusion.....	40
6.2	Recommendation.....	40
REFERENCES	41



LIST OF FIGURES

<i>Figure 1:</i> A: Location of the Orange Basin (red box) along the west coast of South Africa and southern offshore Namibia. B: Satellite imagery of the 3-D seismic survey in the Orange Basin area highlighted by the green box (Kramer and Heck, 2013). VE=vertical exaggeration.....	3
<i>Figure 2:</i> Chronostratigraphy displaying the evolution of the Orange Basin (after McMillan, 2003). The tectonic evolution of the Orange Basin has in this study area been separated into 5 evolution stages namely A to E. These evolution stages are based on the important stages for the basin’s structural evolution leading to the formation of gravity collapse systems.....	4
<i>Figure 3:</i> Chronostratigraphy of the Orange Basin based on the results of seismic interpretation. Lithostratigraphy compiled by de Vera <i>et al.</i> (2010) from Séranne and Anka (2005) and Paton <i>et al.</i> (2008).....	7
<i>Figure 4:</i> Structural evolution of the Orange Basin gravity-driven system (de Vera <i>et al.</i> , 2010).	9
<i>Figure 5:</i> Gravity collapse model for the Niger Delta. The Figure shows the structural evolution of the delta to be similar to the Orange Basin. The Model is separated into three parts. A represents the extensional phase, B is the transitional zone and C is the compressional zone where overpressured shales detached. (After Khani, 2013).....	10
<i>Figure 6:</i> The steps used to interpret the 3-D seismic cube of the Orange Basin	12
<i>Figure 7:</i> The three cross sections illustrate an increase in deformation from the south to the north of the Study area. The cross sections A-A’, B-B’ and C-C’ represent the southern, the start of internal deformation and the northern portion of the Study area respectively.	16
<i>Figure 8:</i> Contour map of horizon 1 and 2. Contour interval is 100ms TWT. The thickness change is between top zone containing deformed sediments and the marker bed containing the thrust faults (seismic facies 1).....	18
<i>Figure 9:</i> Isochron map for horizons 2 and 3. Contour interval is 75ms. The thickness change is for seismic facies 2. Zone A in the north and Zone B in the central part of the Study area have the highest thickness time on the map. Thickness map shows uniform thickness change towards the south.	19
<i>Figure 10:</i> Isochron map for horizon 3 and 4. Contour intervals 50ms. This map shows a uniform change in thickness from zone B to A (red dotted line).....	20
<i>Figure 11:</i> Interpreted seismic horizons displaying seismic facies and faults.	21

<i>Figure 12:</i> The cross section B-B' displays the start of thrust faults while C-C' has the generational listric faults which are counter directional to the thrust faults	23
<i>Figure 13:</i> The Figure above shows: (A) the distribution of automatically extracted fault patches which was interpreted using Petrel [®] 2014 and (B) which shows different zones with faults. The automatic fault extraction (fig.13A) technique allowed for the distribution of fault patches in the Study area. The fault patches create a hemispherical shape from the central eastern part to the western deep part of the Study area. The shallow region (Fig.13A (P)) in the north has a lesser fault concentration as compared to the north western deepening end (Q) of the Study area. There are minor fault patches in the south east (R) and no significant fault patches in the south west (S). Using the fault extraction method the fault slip angle of thrust faults has been estimated to be ~25 degrees.	24
<i>Figure 14:</i> Rose diagrams showing the frequency distribution of dip and strike of faults.	26
<i>Figure 15:</i> The stereographic projection of faults points. Sets 1 illustrate normal faulting while sets 2 and 3 represent thrust faulting.	27
<i>Figure 16:</i> Anderson's fault classification (Yin, 1989).....	28
<i>Figure 17:</i> Schematic representation of the simple (a) and complex impact crater (b, c) formations. (After Osinski, 2005).....	33
<i>Figure 18:</i> Stages for the formation of the meteorite impact. (After Osinski, 2005).....	34
<i>Figure 19:</i> Outward propagation of deformation vectors as the result of a probable bolide impact. Adapted from www.upstreamonline.com and modified after Mhlambi (2014). ..	35
<i>Figure 20:</i> Three-dimensional view of the structure mapped at the base of the Cenozoic strata, adapted and modified from Mhlambi (2014).	36
<i>Figure 21:</i> Automatic fault extraction from Petrel [®] 2014 using 3-D seismic data for this study shows a concentric distribution of faults.....	36
<i>Figure 22:</i> The Figure above shows the interpreted seismic horizons which have been used to understand the geomorphological and structural geometry of the Study area. Seimo-facies 1, 2 and 3 are also depicted.	38
<i>Figure 23:</i> Duplex structure in dolomitic sandstones near Svalbard. Note the horses, floor thrust and roof thrust (after Fossen. 2010).....	39

CHAPTER 1

1. Introduction

The tectonically quiescent passive continental margins may experience a variety of stress states and undergo significant vertical movement post-breakup (Salomon *et al.*, 2014). The development of major faults during oceanic lithospheric extension is more likely caused by mantle plumes intruding on the base of the lithosphere driven by far-field stresses which causes thermal weakening, regional uplift and the development of deviatoric tensional stresses (Ziegler and Cloetingh, 2004).

The economic potential associated with gravity-driven thrust systems has attracted structural geologists and geophysicist for many decades (Tavani *et al.*, 2014). As a result, a large amount of subsurface seismic data on the deformation patterns from gravity induced thrust-related anticlines is available in the literature (Tavani *et al.*, 2014). A study by Jaboyedoff *et al.*, (2013) showed that structures and fabrics formerly interpreted as purely of tectonic origin are instead the result of large slope-deformation, prompting an in-depth look into the mechanism responsible for the development of these structures. This led to the discovery of many inaccurately interpreted tectonic histories of many basins including the Orange Basin. Development of slope failures is progressive through time and space (Jaboyedoff *et al.*, 2013), and recognition of such structures using techniques like paleo-stress analysis and seismic evaluation (which have been applied in this study) can minimise misinterpretations of structural geology of a particular area.

The paleo-stress analysis is applicable to the understanding of gravity collapse systems because of the analogy between gravity faulting and regional tectonics (Baron *et al.*, 2013; Chigira *et al.*, 2013) The paleo-stress techniques require the use of azimuth in rose diagrams and dip and azimuth for stereo-nets to locate the principal stress direction and understand the stress evolution of the area. This in turn allows one to distinguish between compressional and extensional mass-movement stress phases. Structural seismic evaluation techniques allow one to map horizons and faults. Mapped horizons are used to create surfaces. We can use these surfaces to create thickness maps to analyse relative change throughout the area of study. The faults are mapped for tectonic stress field analysis, 2-D reconstruction, to identify zones of weakness and differentiate between deformational domains such as extensional, transitional or contractional domains (Salomon *et al.*, 2014).

The Orange Basin provides exceptional 3-D structures of folds and faults generated during soft-sediment slumping (Butler and Paton, 2010). The evolution of the slump systems, which are gravity-induced, shows a progressive move from initiation, translation, cessation, relaxation and finally the compaction phase resulting in the formation of thrust packages typically seen as piggyback sequences and imbricate faults (Kuhlmann *et al.*, 2010). This slumping and failure is categorized as either: coherent, semi-coherent, or incoherent domains. This classification reflects an increase in deformation and displacement of sediment (Alsop and Marco, 2013).

Initial evaluation of the 3-D seismic data in this area of the Orange Basin shows that there is an increase in the degree of deformational features from the south to north.

1.2 Aims and Objective

This study will present results aimed at describing the degree of the change in deformation across the basin related to gravity tectonics. In order to achieve this, the interpretation will evaluate the 3-D seismic cube to determine thickness change and number of thrust fault. This will then lead to an evaluation of the stress regime in the Study area. The stress field analysis will help better understand the tectonic scale mechanisms driving the gravity tectonics in the Orange Basin.

1.3 Location of the Study area

The Study area is located in the Orange Basin offshore south-western South Africa. The Orange Basin covers an area of approximately 130 000 km² and is located in shallow to deep water with depths between 100-2850 m (Séranne and Anka, 2005; Hirsch *et al.*, 2010; Paton *et al.*, 2008). The Study area covers 8200 square kilometre (km²) and is located approximately 370 km northwest of the Port of Saldanha (Fig. 1). The furthest point to the surveyed area is 370 km offshore (Kramer and Heck, 2013).



Figure 1: A: Location of the Orange Basin (red box) along the west coast of South Africa and southern offshore Namibia. B: Satellite imagery of the 3-D seismic survey in the Orange Basin area highlighted by the green box (Kramer and Heck, 2013). VE=vertical exaggeration

1.4 Tectonic Setting of the Orange Basin

The Orange Basin is the youngest and largest of all the basins in the South African offshore basins (Paton *et al.*, 2008). During Gondwana break-up and the opening of the South Atlantic in the late Jurassic, 8 km thick synrift and drift sedimentary successions were deposited in the Orange Basin (Gerrard and Smith, 1982; Paton *et al.*, 2008; de Vera *et al.*, 2010; Kuhlmann *et al.*, 2010). The tectonic elements that were formed during break-up include the formation of the depo-centre, half-grabens and gravity-induced growth faults (Granado *et al.*, 2009).

The Orange Basin passive-margin accommodation space shows that a single tectonic event resulted in a significant change to both the style and position of sediment accumulation during its post-rift evolution (Paton *et al.*, 2008). The evolution of the Orange Basin passive margin has two stages. The first stage composed of aggradational shelf margin deposits with little or no deformation during the Cretaceous. The Late Cretaceous deposition was punctuated by an episode of margin tilting that resulted in

significant erosion of the inner margin and alteration of the margin architecture. The second stage is categorized by substantial margin instability and the development of a coupled growth fault and toe-thrust system that occurred in the Cretaceous and Tertiary shelf margin (Paton *et al.*, 2008).

1.5 Basin Fill and Evolution

The underlying synrift succession comprises generally isolated and truncated remnants of half-grabens. The thick wedge of drift sediments underwent repeated deformation of the palaeo-shelf edges and palaeo-slopes due to sediment loading and slope instability, especially in the Upper Cretaceous (Kuhlmann *et al.*, 2010).

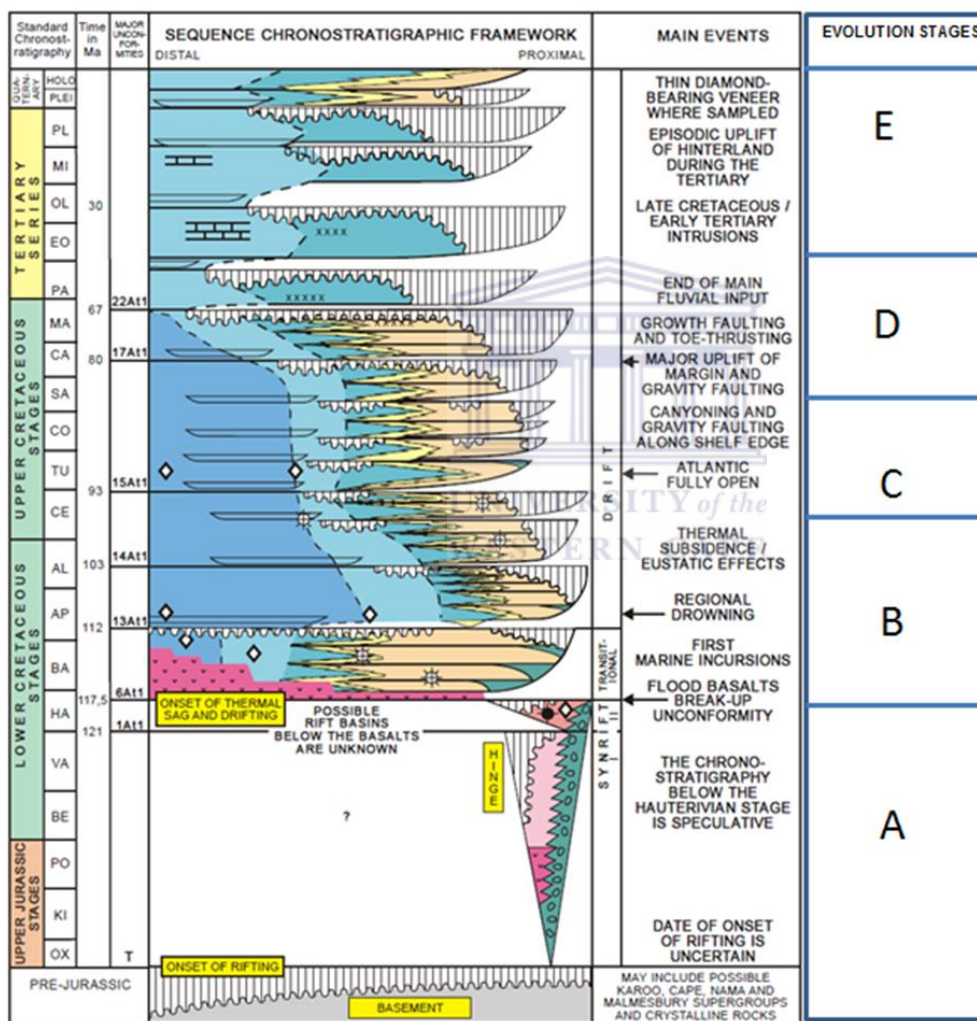


Figure 2: Chronostratigraphy displaying the evolution of the Orange Basin (after McMillan, 2003). The tectonic evolution of the Orange Basin has in this study area been separated into 5 evolution stages namely A to E. These evolution stages are based on the important stages for the basin’s structural evolution leading to the formation of gravity collapse systems.

Prior to the onset of full drift open oceanic conditions there was a deposition of early drift successions which were the proto-oceanic successions consisting of restricted marine and

red continental sediments which are intermittently interposed with basaltic lavas (Fig.2. stage A). During this time mid to late Jurassic north-northwest trending half-grabens and rifting sequences were formed. These rifting sequences were overlain by a 2000-metres-thick Barremian-Aptian aged rift-to-drift transitional sequence (Fig.2. stage B) during the drifting phase. The drift phase successions display progradational stacking patterns with low tectonic and eustatic accommodation (Jungslager, 1999).

The opening of the Atlantic Ocean (Fig2. stage C) resulted in canyoning and gravity faulting along the shelf edge between Turonian and Coniacian ages (Muntingsh, 1993; Jungslager, 1999). The Orange Basin passive margin uplift (Fig2. stage D) resulted in mantle plume and massive denudation which was accompanied by growth faulting and toe-thrusting. The latter mechanisms resulted from gravitational potential energy contrasts and slope instability built up during the Campanian to Maastrichtian depositional epochs (Muntingsh, 1993; Jungslager, 1999; McMillan, 2003).

The late Cretaceous Campanian-Maastrichtian progradational sequences (Fig2. stage D) were deposited as the result of margin uplift, tilting and subsequent erosion of the inner shelf which is clearly shown in the previously interpreted 2-D seismic data (Muntingsh, 1993; McMillan, 2003; Paton *et al.*, 2008). The poorly documented Tertiary to present sediment successions have well-developed siliciclastic sedimentary wedges which increases in thicknesses basinward and ranges between 200 to 1500 metres thick (Fig2.E). A major tectonic event between Tertiary and present is the Miocene episodic uplift.

The phases for the evolution of the Orange Basin according to Hirsch *et.al*, (2010) are summarized below.

- Rifting phase which composed of pre-rift successions (older than Late Jurassic, >130 Ma) that is overlain by syn-rift deposits of Late Jurassic to Hauterivian age (121-116.5 Ma) (Fig2.A)
- Early drifting phase which stretches from late Hauterivian to the Barremian-early Aptian depositional epoch (Fig2.B)
- Drifting phase which is occupied by sediments of Aptian age (113- 108 Ma) to the present day successions (Fig2.C-E). This phase composed of the Cenomanian-Turonian anoxic event and a thick sedimentary wedge with slump structures and toe thrusts.

CHAPTER 2

2. Literature Review

Gravity collapse systems are characterized by broad down-dip contraction tectonics and up-dip extension tectonics that are linked by one or more weak detachment layers. These systems of deformation typically comprise of basinward vergent thrust imbrication associated with folds, which usually does not occur until there is sufficient overburden facilitated by high fluid pressures (de Vera *et al.*, 2010). The understanding of the impact of gravitational tectonics is the key to evaluate lateral compaction in deep-water fold and thrust belts because they indicate significant amount of deformation that is not accounted for in the imaged thrust belt structure (Butler and Paton, 2010).

The Orange Basin has gravity driven system with extension above the submarine slope and contraction towards the toe of the slope (Paton *et al.*, 2008). The gravity driven system is responsible for the detachment and thrust faulting distribution which has altered the thickness of sedimentary layers in the Orange Basin (de Vera *et al.*, 2010; Butler and Paton, 2010). The gravitational tectonics of the Orange Basin has been well documented; however the large scale driving mechanisms are poorly understood. Using the recently acquired 3D seismic data of this area, this study will contribute to the understanding of large-scale tectonic processes associated with gravity collapse systems of a passive continental margin.

2.1 Previous Studies

2.1.1 Regional Seismic Stratigraphy of the Orange Basin

A more recent study on the 2-D regional seismic stratigraphic interpretation of the Orange Basin was conducted by de Vera *et al.* (2010) which is based on the work by Séranne and Anka (2005) and Paton *et al.* (2008). This 2-D seismic interpretation divided the seismic stratigraphy of the Orange Basin in two megasequences (Fig.3): (1) The Synrift Megasequence and (2) The Post rift Megasequence.

2.1.1.1 Synrift Megasequence

Deposition of the Syn-Rift Megasequence is between late Jurassic and late Hauterivian (160-127 Ma) with low frequency continuous to discontinuous seismic reflections with fanning geometries and basin-ward dipping high amplitude reflectors (Fig.3). During the late to early stages of continental rifting volcanic wedges were deposited (Séranne and

Anka, 2005). These volcanic wedges are now reflected and interpreted as seaward dipping reflectors.

2.1.1.2 Post rift Megasequence

The Post-Rift Megasequence consists of a late Hauterivian to present day depositional sequence (Fig.3). A Late Hauterivian break-up unconformity (ca. 127 Ma) separates Post-Rift Megasequence from the seaward dipping reflections of the Syn-Rift Megasequence. de Vera *et al.* (2010) subdivided the Post-Rift Megasequence in five distinct depositional sequences referred to as Post-rift sequence I-V.

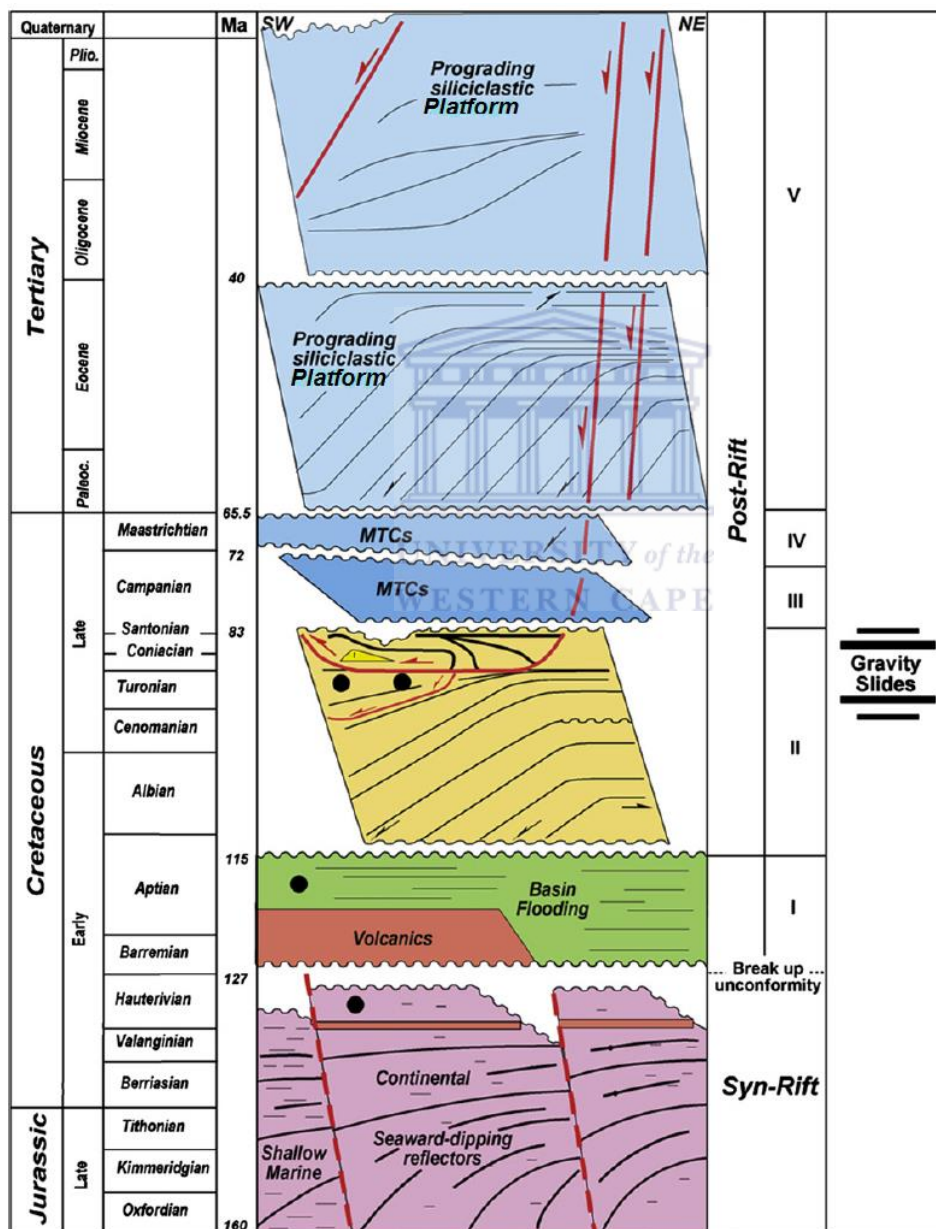


Figure 3: Chronostratigraphy of the Orange Basin based on the results of seismic interpretation. Lithostratigraphy compiled by de Vera *et al.* (2010) from Séranne and Anka (2005) and Paton *et al.* (2008)

Post-rift seismic sequence I unconformably overlies the Syn-Rift Megasequence of Barremian-Upper to Aptian age (Fig.3). Post-rift II is of Upper Aptian to Santonian age and includes the gravity-driven systems of the Orange Basin. Post-rift seismic sequence II is overlain by post rift sequence III which is of Santonian-Campanian age and deposited on the outer continental shelf.

Post-rift seismic sequence III is unconformably overlain by Post-rift IV which stretches from late Campanian to Maastrichtian and is characterized by mass transport complexes (MTCs). Post-rift seismic sequence V is characterized by a basin-ward shift of siliciclastic platform sedimentation with well-developed prograding clinoforms. Post-rift seismic sequence V was deposited between the present day and the base of Tertiary (65 Ma).

Generation of hydrocarbons during the Late Cenomanian to Early Turonian source rocks (Fig.3) reduced friction at the base of the slide and enhanced the efficiency of the shale detachment faulting (Muntingh and Brown, 1993; Séranne and Anka, 2005; Ezekiel *et al.*, 2013; de Vera *et al.*, 2010). The interpretation by Séranne and Anka (2005) and de Vera *et al.*, (2010) puts gravity sliding in Post-rift II sequence between the Turonian and the Coniacian occurring only during these two periods. The interpretations by Muntingh (1993), Jungslager (1999) and McMillan (2003) suggested that massive gravity faulting in the Orange Basin occurred in the Turonian-Coniacian and also in the Campanian-Maastrichtian depositional epochs.

The opening of the Atlantic Ocean during Gondwana started from the north and continued towards the south (Kuhlmann *et al.*, 2010). Late Cretaceous rifting resulted in the separation of the South American and African plates and generated accommodation space in the form of grabens and half-grabens in the Orange Basin. This late Cretaceous structural change resulted in highly aggradational deposition which resulted in the development of a complex zone of slumps, rollover anticlines and tilted fault blocks (Brown *et al.*, 1995).

2.1.2 Gravity-driven Systems of the Orange Basin

The episodic gravitational collapse system of the Orange Basin margin characterizes the mid and late Cretaceous Period deformation. de Vera *et al.* (2010) suggested that structural evolution of the Orange Basin gravity-driven system is short-lived spanning from the Coniacian (ca. 90 Ma) to the Santonian (ca. 83 Ma) Epochs.

Jungslagger (1999) and Paton *et al.* (2008) reported that gravity sliding also occurred during the late Cretaceous Period. Their interpretation of the Orange Basin extends the period for the formation of the gravity collapse system to Cenomanian and Maastrichtian Epochs. Many studies on the Orange Basin attribute that gravity-failure in the late Cretaceous Period occurred because of differential sedimentary loading associated with rapid delta progradation related to high sedimentation rates (Jungslagger, 1999; Paton *et al.*, 2008). Butler and Paton (2010) suggested that gravity failure can also occur as result of the presence of an efficient, commonly over-pressured detachment layer.

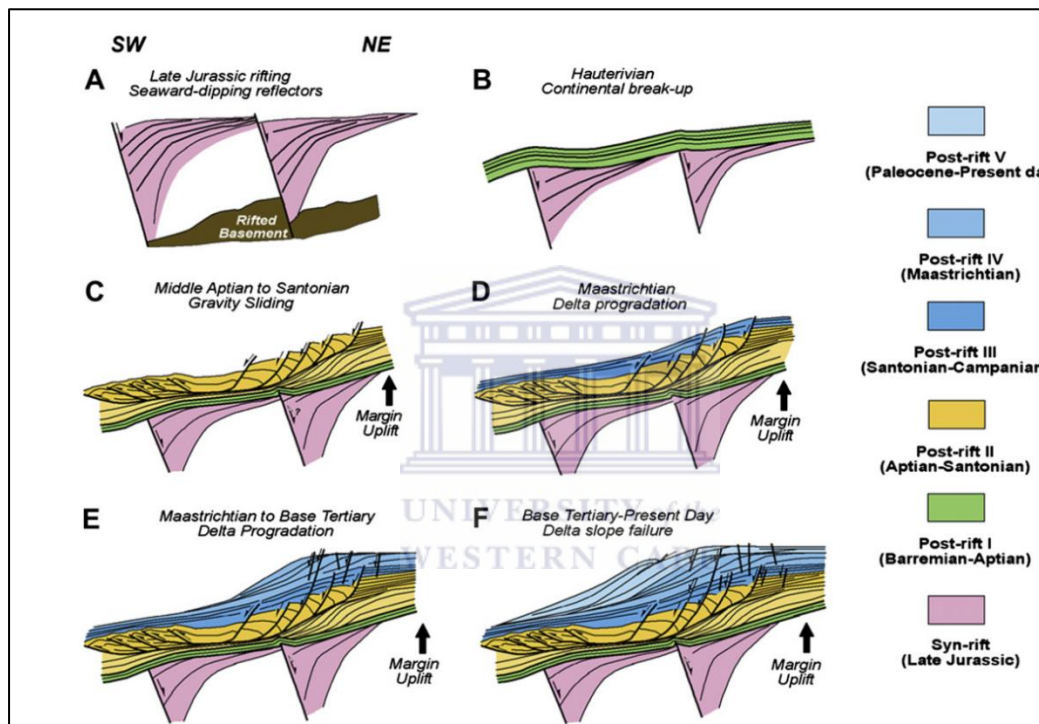


Figure 4: Structural evolution of the Orange Basin gravity-driven system (de Vera *et al.*, 2010).

As stated above, the gravitational collapse system of the Orange Basin is estimated to have developed between the Cenomanian (ca. 100 Ma) and the Campanian (ca. 80 Ma) and to a lesser degree during Maastrichtian (ca. 70 Ma) (Fig.2.A-E) Epoch. Orange Basin margin evolution started with rifting during the late Jurassic which is represented by well-imaged wedges of seaward-dipping reflectors (Fig.4A). The Post-rift Megasequence was deposited, starting with a deepening-upward succession of continental to deep marine sediments during the Hauterivian (Fig.4B).

The combined effect of post-rift thermal subsidence and passive margin uplift 100 to 80 Ma ago initiated gravity failure resulting in stacked gravity slides with complex three-

dimensional geometries (Fig.4C). Gravitational spreading and failure of the margin as the result of high sedimentation rates and delta progradation decreased in Campanian times but the margin uplift continued (Fig.4D). Margin uplift is demonstrated by deposition of a series of prograding clastic wedges (Fig.4E). Sedimentation progradation accompanied by development of extensional faulting and shallow failures continued through Tertiary until present (Fig.6F).

2.2.3 Comparison of the Orange Basin with other gravity collapse systems

There are numerous gravity collapse systems which could be compared to the ones in the Orange Basin like those in the Niger Delta and the Mississippi Delta. The work on and interpretation of gravity collapse structures in the Mississippi Delta has been focused on the loose sediments on the continental margin or deltaic setting (Hersthammer and Fossen, 1999) which is not within the scope of this project. Judging from the seismic data for this Study area, it is concluded that the tectonic history of the Niger delta is comparable to the one in the Orange Basin.

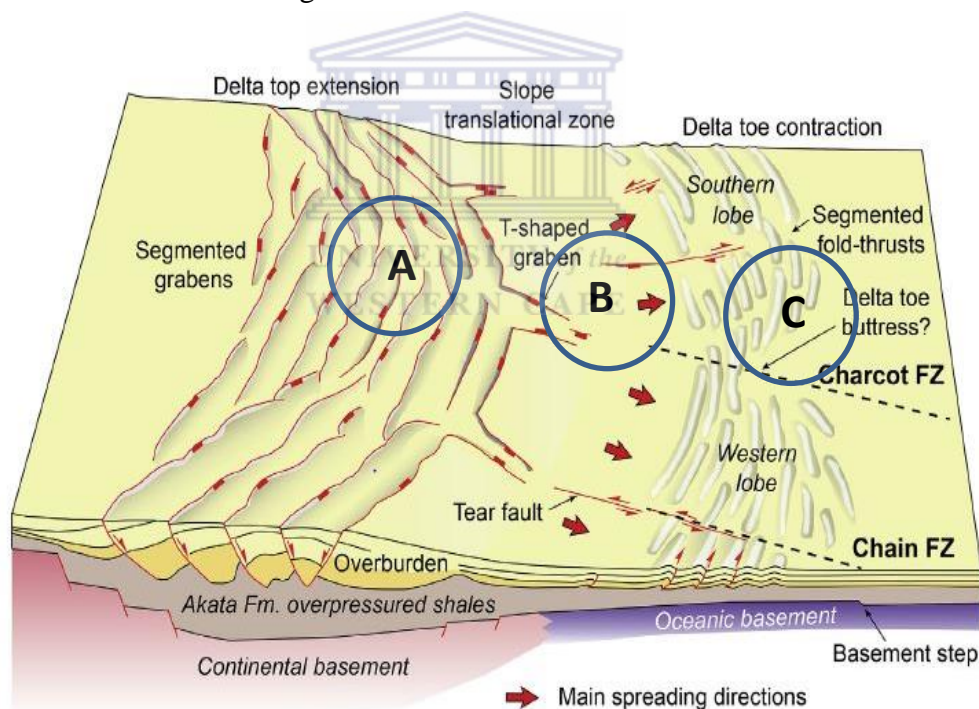


Figure 5: Gravity collapse model for the Niger Delta. The Figure shows the structural evolution of the delta to be similar to the Orange Basin. The Model is separated into three parts. A represents the extensional phase, B is the transitional zone and C is the compressional zone where overpressured shales detached. (After Khani, 2013)

The Niger delta has contrasting structural styles as compare to the Orange Basin. The Niger delta shows structural styles related to low strength detachments while the Orange

Basin indicates a comparatively strong frictional detachment (Butler and Paton, 2010). This comparability between the Orange Basin and the Niger Delta is illustrated through the recent work by Maloney *et al.*, (2012) and Khani (2013) using 3D seismic data. Work by Maloney *et al.*, (2012) demonstrated that the Niger Delta's gravity driven system has a basinward dipping extensional system with one listric master fault plane.

The extensional system creates detachment faulting that switches from a deeper compressional system to a shallower extensional domain similar to the Orange Basin. 3D seismic reflection data was used in these collapse systems to investigate the architecture of the Niger Delta. This study discovered that detachment faulting transfers hanging wall rocks into the footwall, branching off pre-existing detachment levels along zones of mechanical weakness, thus altering the apparent thickness of sedimentary packages (Khani, 2013). Differential sedimentary loading in the Niger Delta played a critical role in causing gravity distribution along with the basin subsidence but in the Orange Basin the deltaic progradation stopped the gravity sliding.

2.2 Problem Statement

The interpretation of gravity collapse structures of the Orange Basin have not given satisfactory answers on the deformational structures observed in the 3-D seismic data. A well-established deformational model can improve structural integrity which can be used to explain how the Study area has been differentiated into curvilinear listric faulting, localized thrusting, lateral compaction and ductile deformation. So to better understand the origins of the deformational features in this Basin, this study aims to focus on the following questions:

1. What is the development in deformation from the south to the north?
2. What are the factors which influenced observed apparent thickness variations?
3. How can a compressional regime coincide within an extensional environment?

CHAPTER 3

3 Methodology

3-D seismic reflection data for this study covers 8200 square kilometre. This 3-D seismic data was interpreted in the Petrel[®] 2014 software and the 2D MOVE[™] software was also used for structural analysis. The seismic data has been provided by Shell Exploration and Production Company to the University of the Western Cape.

Workflow

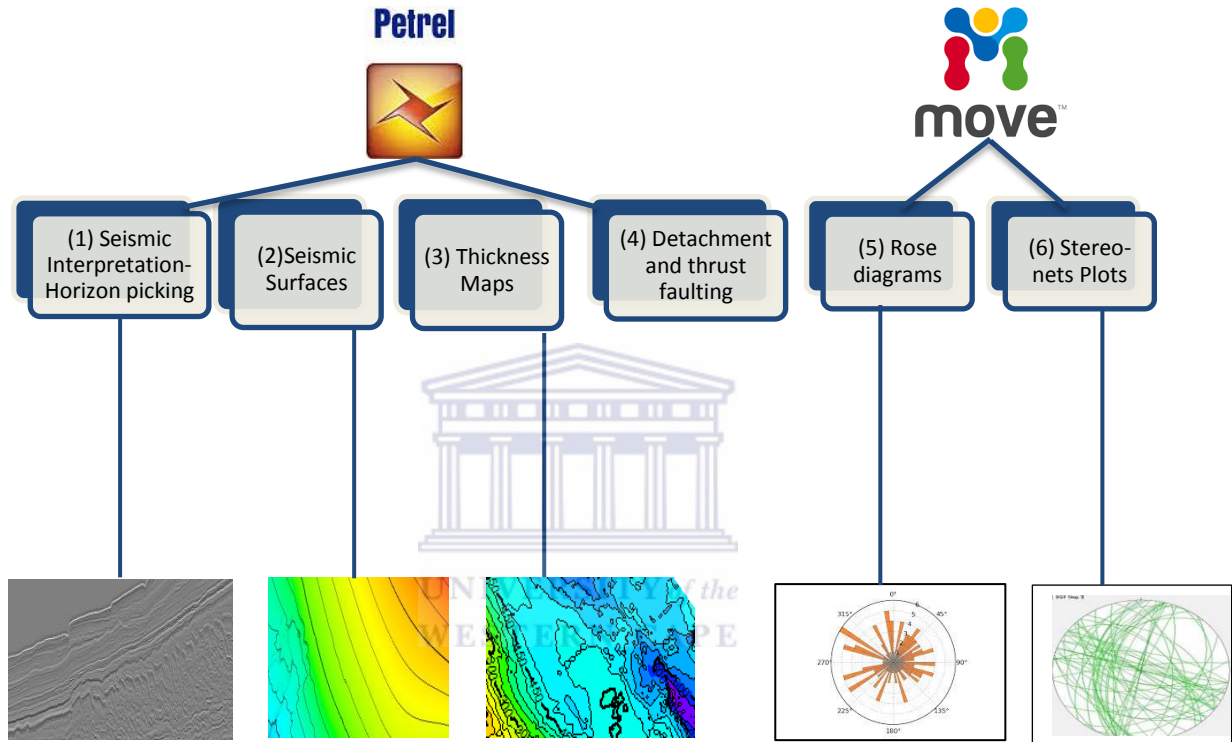


Figure 6: The steps used to interpret the 3-D seismic cube of the Orange Basin

Interpretation of seismic data was as follows: (1) Using the imported seismic data four seismic horizons were mapped using “2-D seeded and manual corrections” interpretation. The four interpreted seismic horizons were interpreted solely based on prominent horizons affected by thrust faulting or gravity collapse structures. (2) Stratigraphic surfaces were created from mapped horizons. (3) Thickness maps (isochron maps) were then extracted from the seismic surface created. Interpretation of changes in depositional activity, stratigraphic evolution and structural growth history through time and space were analysed using isochron maps.

(4) Thrust faulting in the Study area was interpreted using fault dip and dip azimuth. Fault dip and -azimuth were extracted from the seismic cube to analyse thrust faulting and its implication on the stress field distribution. To perform the interpretation of faults, the

following steps were taken. (4.1) Using the realized seismic cube, an amplitude map was created. (4.2) then structural smoothing of the seismic cube were applied. (4.3) a variance or discontinuity cube was generated which (4.3) was then used to perform ant-tracking. Ant-tracking traces all the zones of weakness in the seismic data by searching for discontinuities in the seismic data. (4.4)The automatic fault extraction facility was used to extract fault patches (which are merely fault points with x, y and z coordinates).

Interpretation of the stress field distribution require the use of fault points from interpreted major faults to understand the transition of principal stress direction from south to north of the Study area.

The fault points were extracted from Petrel[®] 2014 in x, y and z coordinates. These fault points were extracted to estimate the dip and dip azimuth from them. The dip and dip azimuth estimated were loaded to the 2D Move[™] software to get orientation of the faults. To understand the structural regime of the area, the fault points which had been loaded in the 2D Move[™] software were plotted in rose diagrams and stereo nets to estimate the fault dip and dip direction. This understanding can help predict the dominant deformational regime which is responsible for most of the observed structural features. Full description for these diagrams can be found in the chapter 4 below.

Fault interaction, as well as any sedimentary layering, does not represent the true stress field because of the limitation of data, so the assumption or prediction of the stress field and deformational regime is likely to be an approximation only.

CHAPTER 4

4 Results

This chapter describes the observed seismic patterns and structural features. The analysis of the seismic data in this chapter presents several approaches employed and the outcomes achieved by interpreting the 3-D seismic data. The interpretation for this study was focused on the following topics:

- 4.1 Seismic Analysis
- 4.2 Thickness extraction
- 4.3 Thrust Faulting
- 4.4 Rose diagrams
- 4.5 Stereo-nets

4.1 Seismic Analysis

4.1.1 Introduction

The 3-D seismic data that have been provided had to be interpreted without the assistance of well data, biostratigraphy data and logs as these were not provided by the company concerned restricting one from assigning the chronostratigraphic age to the interpreted horizons. Using the 2014 Petrel[®] software, five horizons were recognised. These seismic horizons are defined as follows: the seafloor, top of zone containing deformed sediments (green line in Fig.7), marker bed defining thrusts and detachment faults (marked in purple line or squares), base of the zone containing the thrusts and detachment faults (marked in white on Fig.7) and bottom boundary of zone containing deformed sediments (marked in orange on fig.7). These interpreted horizons (with the exception of the seafloor) were separated into three seismic facies (seismic facies 1, 2 and 3) based on the degree of deformation seen.

Seismic facies in turn were interpreted based on internal reflection geometry, nature of the bounding surfaces, amplitude and continuity. The second horizon interpreted after the sea floor was the prominent horizon on top of thrust faulting. The three seismic facies identified are shown in Figure 7. Seismic facies, coupled with the identification of key horizons, were used to separate the Study area into three deformational domains (extensional, transitional and compressional domains) which are discussed later in this chapter.

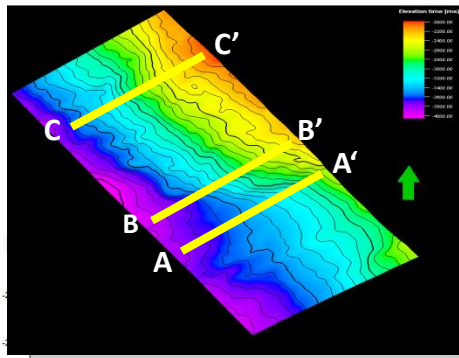
The seismic facies which have been interpreted for the Study area are characterized by subparallel reflections in the south and divergent reflections in the north. The reflections correspond to the impedance contrast of geological entities. The red reflectors are hard events and the blue reflectors are soft events. The gravity deformation is constrained between the top (in green) and bottom (orange) interpreted horizons (fig.7).

4.2 Horizon Interpretation

The seismic facies in cross section A-A' (fig.7) are laterally continuous with little or no deformation. The thrust faulting has not been observed in this cross section. Looking at the top of deformation seismic surface map (Fig.7), the south is relatively shallow and the contours are flattened, no deformation is observed within the interpreted successions. Seismic facies 1, 2 and 3 have a subparallel configuration with continuous seismic reflection patterns and high to medium amplitude.

Cross section B-B' has many deformational features when compared to cross section A-A' that shows no deformation. Cross section B-B' was chosen because it reveals the start of deformation and shows that thrust faulting progresses towards the north of the Study area. Thrust faulting creates discontinuous seismic reflection patterns. This discontinuous pattern is formed by stacking of a single seismic interval which forms as the result of the horses or thrust faults which are numbered as A, B, C, D, E and F (Fig 7b).

Horse A represents the first sign of thrust faulting that stacks on top of horse B. Deformation intensifies towards the east of the cross section forming wedge shaped geometries for horse B to E. Thrust faulting F is less tilted and is followed by a westward decrease of deformational features. This cross section (B-B') has deformational features which alter the thickness of the seismic facies. Seismic facies 1 shows a decrease in thickness towards the west as the thrust faulting intensifies in the same direction. Seismic facies 2 has a landward (eastward) thickening sequence.



Cross sections showing an increase in Deformation from South to North

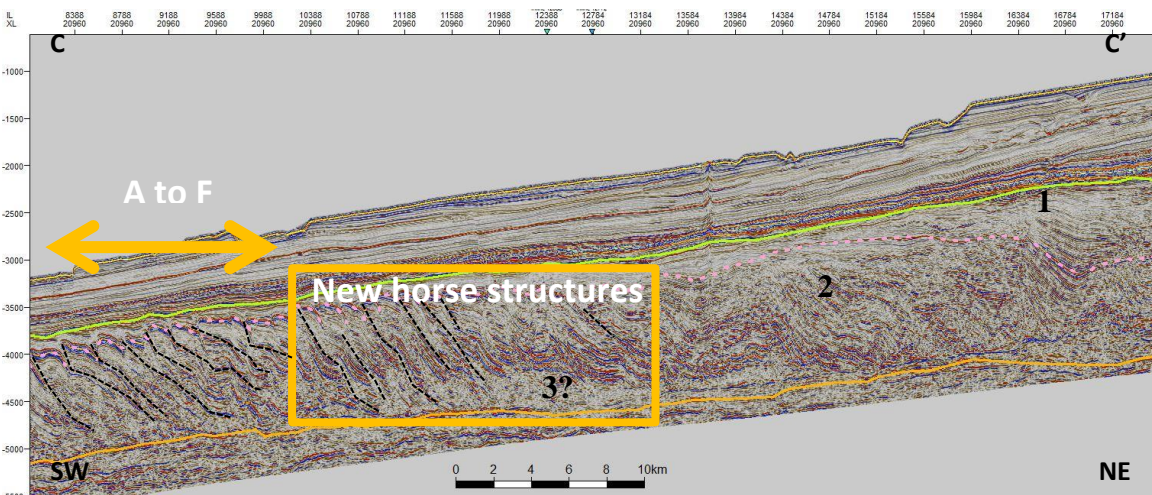
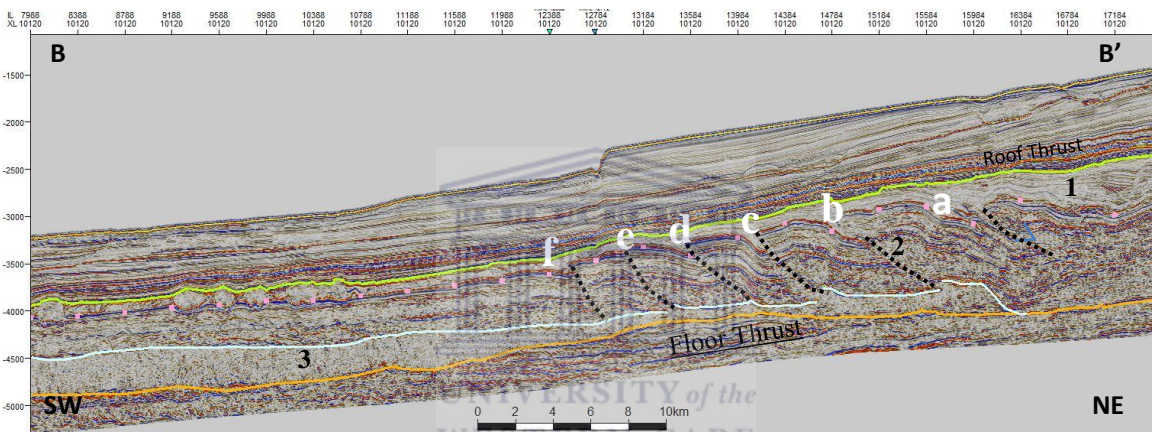
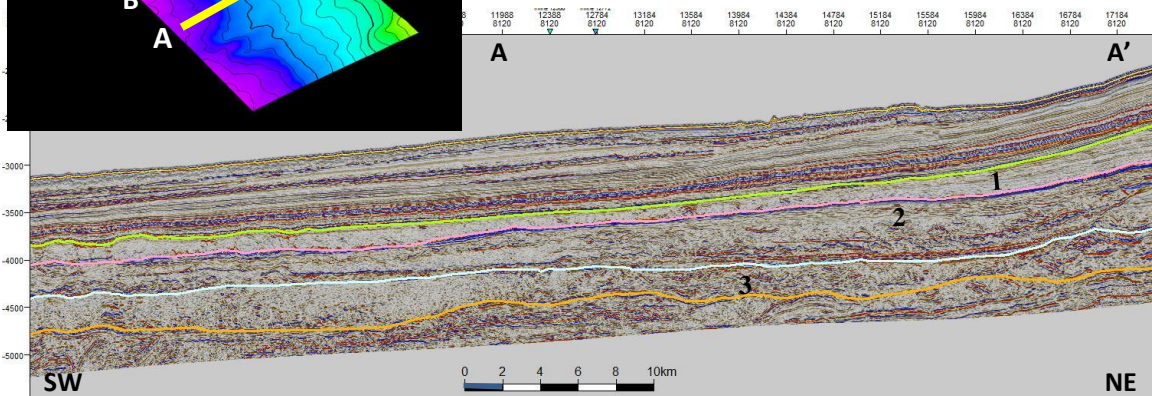


Figure 7: The three cross sections illustrate an increase in deformation from the south to the north of the Study area. The cross sections A-A', B-B' and C-C' represent the southern, the start of internal deformation and the northern portion of the Study area respectively.

Cross section C-C' shows discontinuous seismic configuration with high to medium amplitude within the interpreted horizons. The thrust faulting in seismic facies 1 (in the east of the cross section) is characterised by a divergent configuration defining a wedge-shaped unit. Seismic facies 1 laterally thins westwards as the result of pinching-out of sedimentary packages. Horizons A-F have been rotated and pushed further to the west by generational listric faults adding new thrust faults in seismic facies 2. The top of Seismic facies 2 is pushed closer to the top of sequence 1, making sequence 2 to progressively thicken in the westerly direction. There is no evidence of the involvement of Sequence 3 in cross section C-C'.

4.3 Thickness extraction

4.3.1 Introduction

Thickness maps were extracted to study the basin geometry and topographic relief at different levels of interest. Thickness maps are created from the two seismic surfaces of interest to show the change in thickness throughout the 3-D seismic cube. These maps show change in thickness because of topographic contrast as a result of geological events. Since no well and log data is provided to perform depth conversion, the thickness map extracted are in two-way time (TWT). The well and log data provides check-shot data which is important for velocity modelling which is used to perform depth conversion. Therefore, the thickness discussed in this chapter is a relative thickness represented in two way time (TWT). Isochron (thickness) maps were extracted to understand the relative change in thickness and how changes in structural regime during gravity tectonics control the resultant seismic facies.

Interpreting the thickness change in TWT is not always helpful because TWT does not always translate to true thickness because of many factors that might affect the time for the reflected seismic wave to return to the recorder. Factors that could affect TWT are density and velocity of the material because of poorly consolidated sediments, fluid saturated successions, rock pressure and fluid content among many others (Pandey *et al.*, 2013). Structural uncertainty intrinsic in time is removed through depth conversion to verify the structures of the observed seismic data (Pandey *et al.*, 2013).

4.3.2 Isochron Maps

Isochron maps have been generated between the mapped horizons to interpret structural growth of high and low points of the Study area through time and space. Isochron maps were generated between horizons 1-2, 2-3 and 3-4 (fig.11).The thickness change between

these horizons have been chosen in order to identify the gravity collapse features. High TWT represent an increase in thickness because there is greater separation between the two seismic horizons conversely low TWT represents a lower thickness between the mapped horizons.

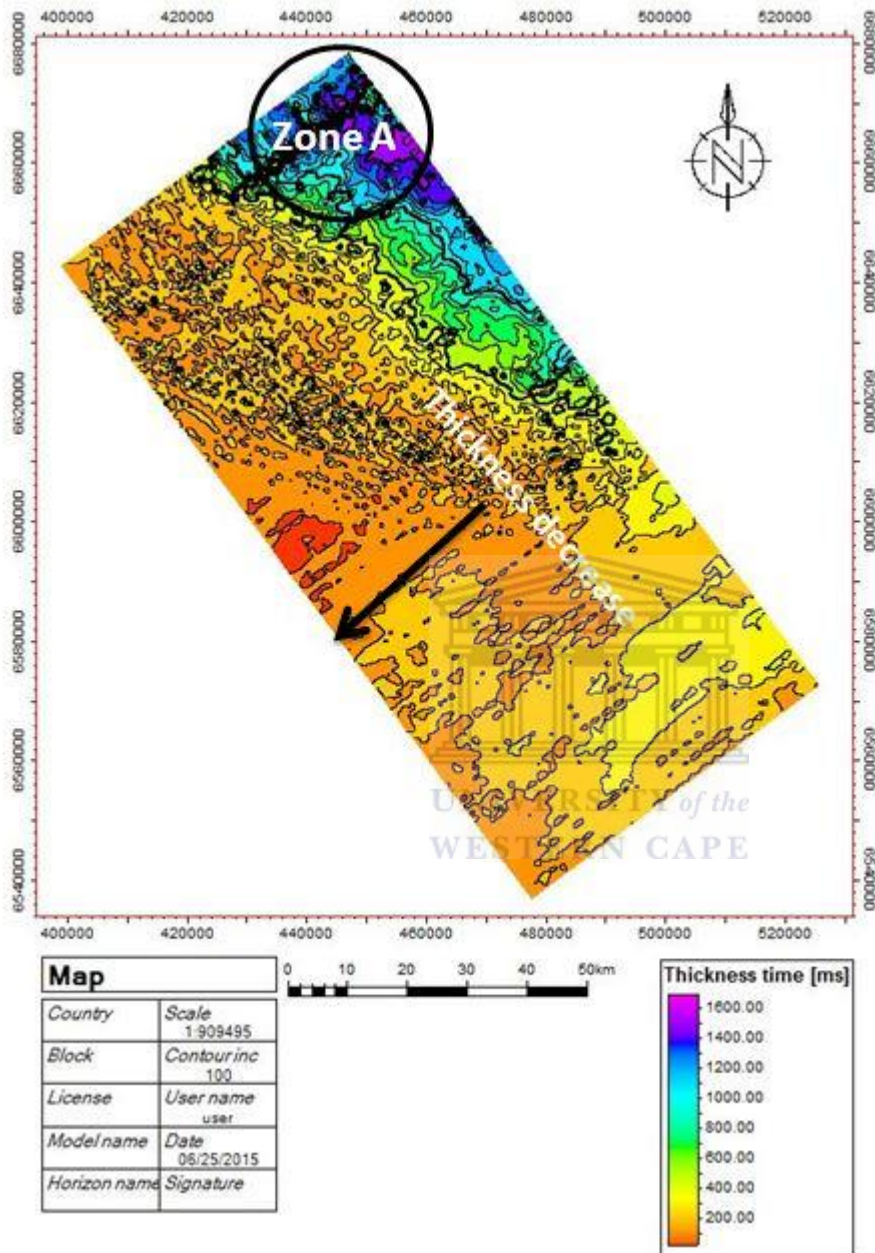


Figure 8: Contour map of horizon 1 and 2. Contour interval is 100ms TWT. The thickness change is between top zone containing deformed sediments and the marker bed containing the thrust faults (seismic facies 1).

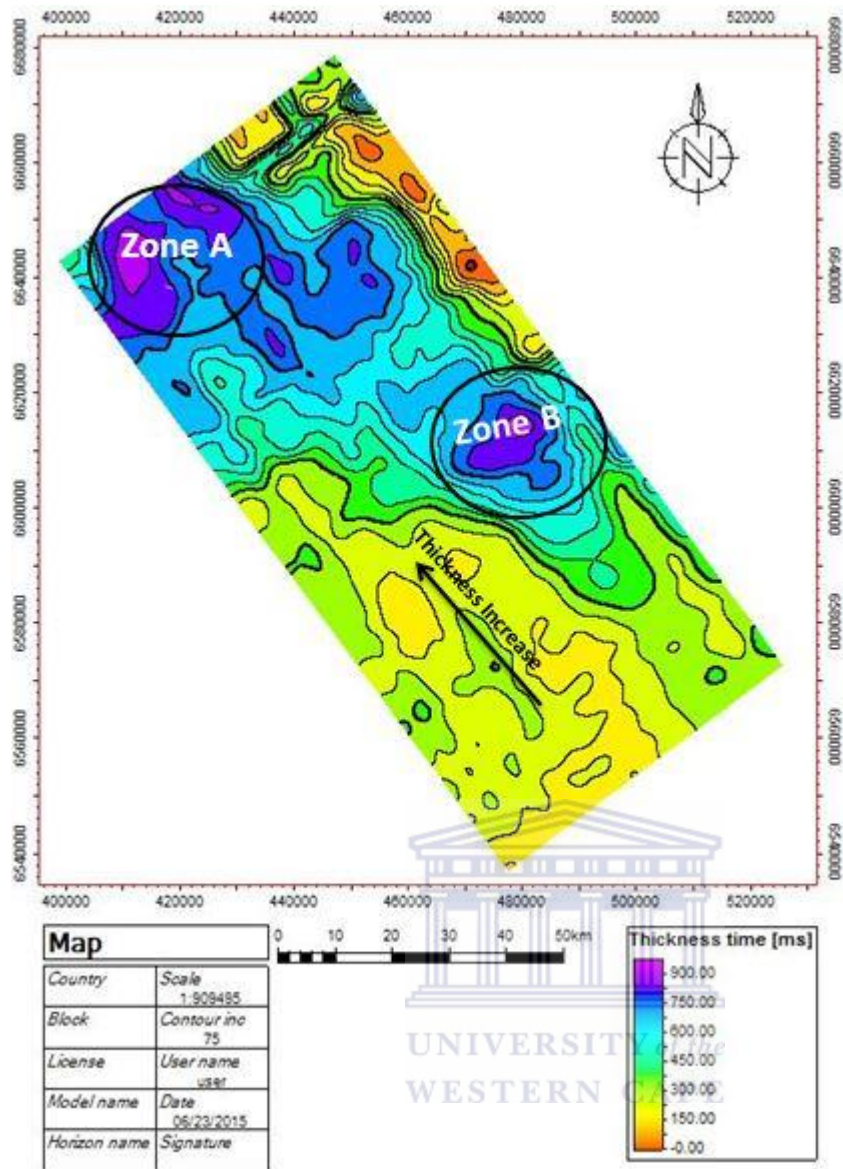


Figure 9: Isochron map for horizons 2 and 3. Contour interval is 75ms. The thickness change is for seismic facies 2. Zone A in the north and Zone B in the central part of the Study area have the highest thickness time on the map. Thickness map shows uniform thickness change towards the south.

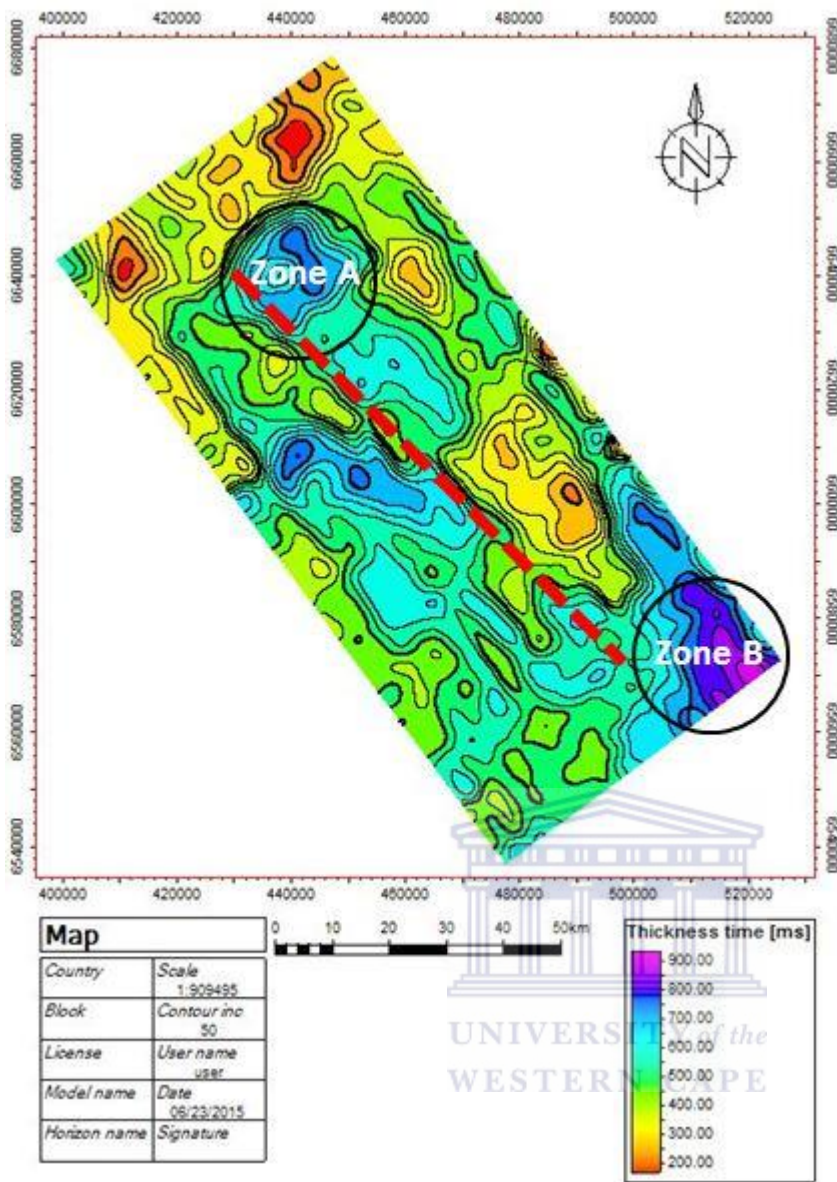


Figure 10: Isochron map for horizon 3 and 4. Contour intervals 50ms. This map shows a uniform change in thickness from zone B to A (red dotted line).

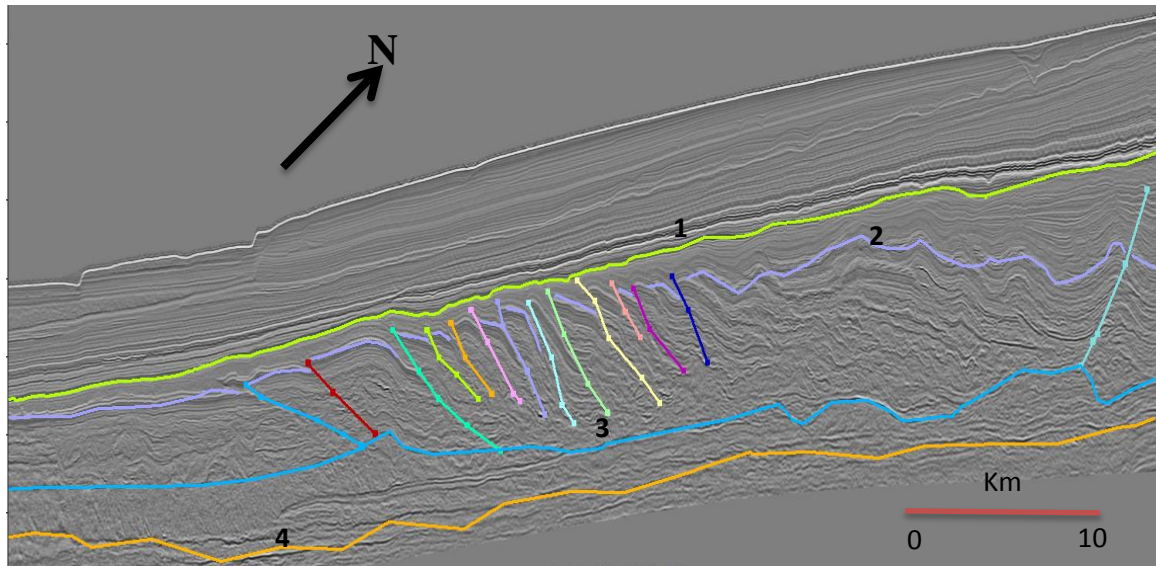


Figure 11: Interpreted seismic horizons displaying seismic facies and faults.

There is a greater separation distance for the horizons in the east as compared to the separation distance in the west, implying that there is lower thickness or less thickness time between the mapped horizons in the western part relative to the thickness variation in the east. **N.B:** The numbers on top of the horizons represents the horizon numbers.

Horizon 1 and 2: The average TWT thickness time for the northern part in Figure 8 is 1350 milliseconds (ms) while the average in the south is approximately 150ms. Thickness of this interval varies from ~100ms to ~1600ms. The thickness increases towards the north eastern side, while in the south western part of the Study area a thickness decrease is observed. The short distance between Horizon 1 and 2 (fig. 11) makes it easier to for one to observe why the thickness changes greatly from the north to the south of the area. Zone A in the centre has an average thickness of ~1350ms. The north east of Figure 8 corresponds to the wedge seismic units from cross section-C-C' (fig. 7) which was created by NW-SE trending thrusting forming horses. The western side of the isochron map shows contours that are far apart meaning the rocks are flat lying.

Horizon 2 and 3: Average sediment thickness (fig.9) in south western side is ~225ms and it gradually increases towards the north eastern side with an average thickness ~750ms in zone B and ~900ms for zone A. Fig.9 shows a north westwards thickness increase different from Figure 8. The contours in the south western part of the Study area are flat and far apart as compared to the contours in zone A and B where there is a larger thickness change.

Horizon 3 and 4 thickness map: The isochron map in Figure 10 has a thickness interval which varies from ~150 to 950ms. Sediment thickness change is relatively homogeneous towards the centre of fig.10 with an average thickness of ~550ms. The structural highs and lows affect the separation distance between the mapped horizons by either decreasing or increasing the thickness change. A better understanding of thickness change which has been explained in the Figure 8, 9 and 10 can be obtained by using the number of thrust faults. The thrust faults create structural highs which reflect thickness variations in isochron maps.

4.4 Thrust faulting

The thrust faulting creates discontinuities along the interpreted seismic horizons which becomes chaotic as the deformation intensifies. Thrusted seismic horizons are constrained between horizons 1 to 4 (see Fig.7 and 11 above). Figure 7 shows that deformation starts with three thrust faults (cross section B-B' see fig.12) and increases to eight thrust faults or horses (cross section C-C') for every 10 km laterally. The thrust faults are initiated in the southeast and progressively increase in number towards the north. The number of thrust faults increase laterally forming many horse structures. These horses represent westward verging, rotated and landward dipping thrust faults in deep and shallow regions of the Study area.

The listric faults continue parallel along the bottom orange horizon (fig.12). The transition zone from extensional to compressional faulting shows fault-fold propagation with a wavy reflection pattern indicating an onset of thrust faults (fig.12, C-C'). The integration between normal and thrust faults forms imbricate structures (cross section B-B'). The average horizontal separation distance from one thrust to the next is ~500m.

Cross section B-B' shows imbricated thrust faults and curvilinear normal faults in the west and east of the seismic profile respectively. The separation distance between the normal fault and the thrust fault system is ~14 km. The onset of antithetic faults creates wedge shape seismic units in the east which increases the thickness of seismic facies 1 while reducing the thickness of seismic facies 2 and 3. The faults trending northeast-southwest (fig.12, cross section B-B') which are counter directional to the gravity and toe-thrust faults, form an internal downlap. The fault geometry of cross section C-C' shows a rotated thrust fault block. Seismic facies 1 and 2 in cross section C-C' are discontinuous and chaotic. The deformation also consists of growth structures, stair-case faults and piggy-back structures. Concordant and subparallel seismic patterns of the south do not have significant deformational features, so they have not been illustrated.

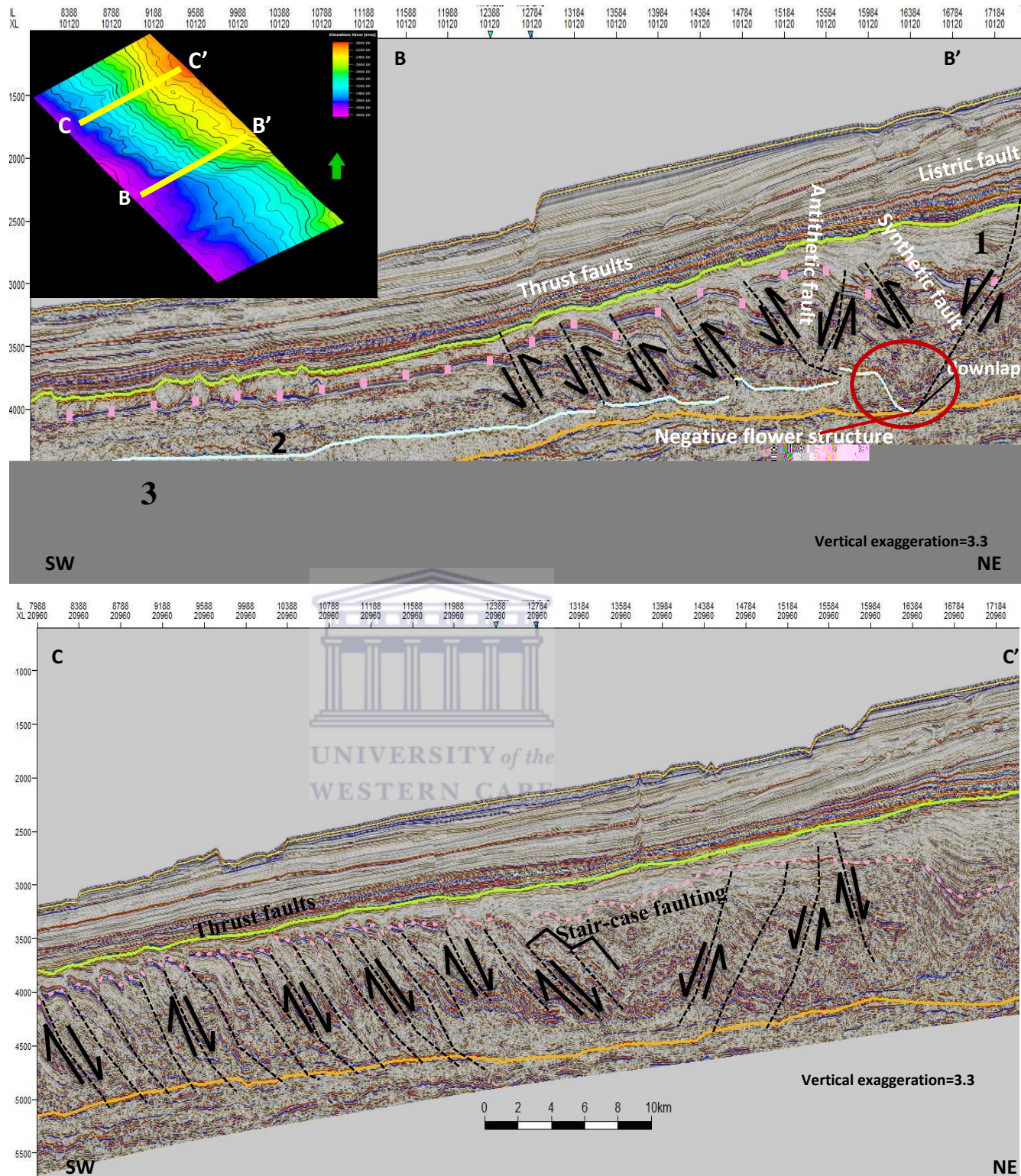


Figure 12: The cross section B-B' displays the start of thrust faults while C-C' has the generational listric faults which are counter directional to the thrust faults

North westward directed fault distribution of the Study area

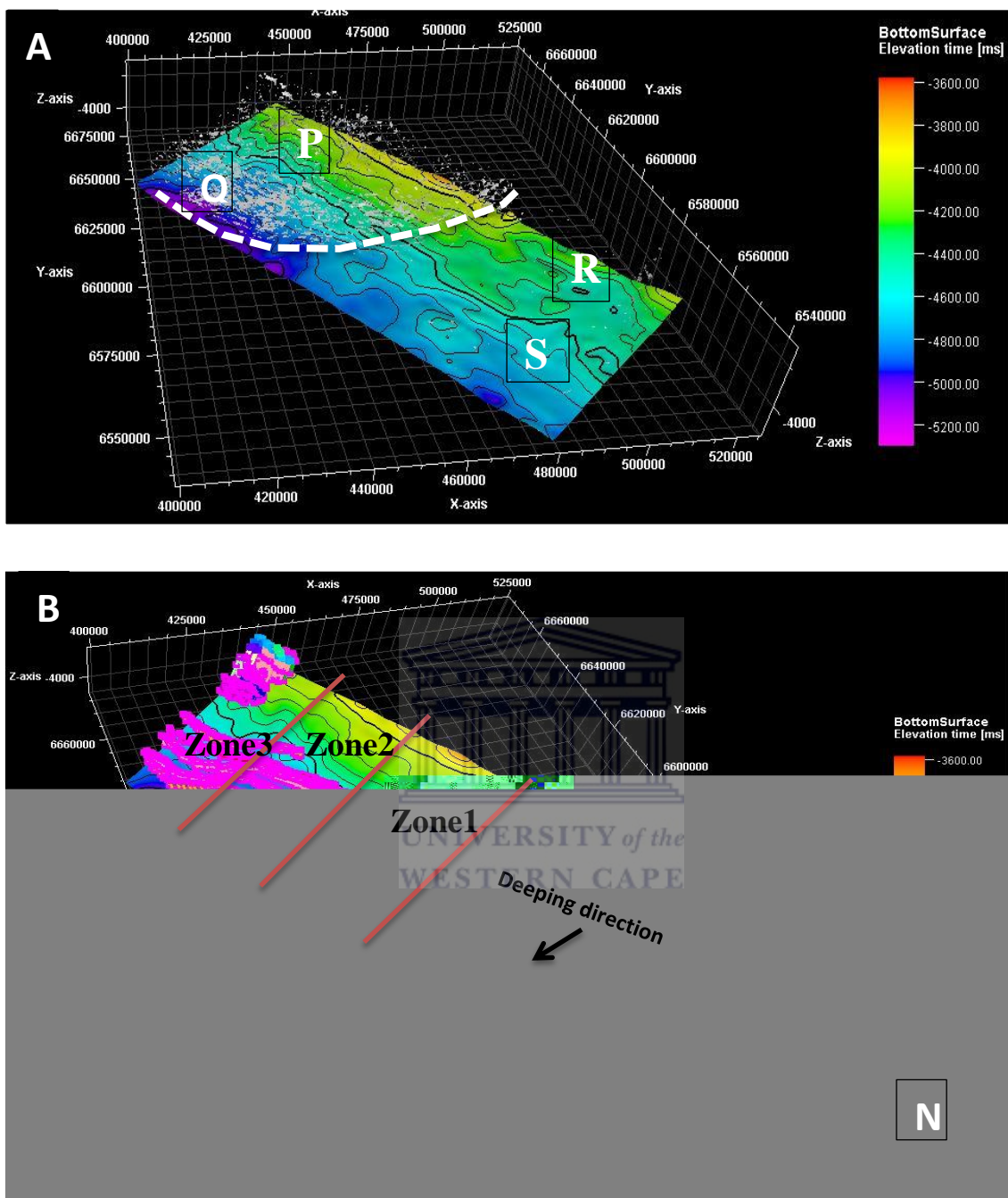


Figure 13: The Figure above shows: (A) the distribution of automatically extracted fault patches which was interpreted using Petrel[®] 2014 and (B) which shows different zones with faults. The automatic fault extraction (fig.13A) technique allowed for the distribution of fault patches in the Study area. The fault patches create a hemispherical shape from the central eastern part to the western deep part of the Study area. The shallow region (Fig.13A (P)) in the north has a lesser fault concentration as compared to the north western deepening end (Q) of the Study area. There are minor fault patches in the south east (R) and no significant fault patches in the south west (S). Using the fault extraction method the fault slip angle of thrust faults has been estimated to be ~25 degrees.

The Figure displays different zones based on the interpreted faults of the Study area. The majority of the faults are concentrated in zone 3. Fault slip points are very few in the south and have no specific trend and orientation but the north part has a significant fault concentration. The separation of the Study area into different zones shows an increase in faults from the internal (zone 1-2) to the end (zone 3) of the area of study.

4.5 Rose Diagrams Orientation

4.5.1 Introduction

Rose diagrams are circular frequency histograms that are used for directional (azimuthal) data. The Figures below show that the fault azimuth frequencies are counted in 30 degree azimuthal bins. Rose diagrams display the frequency of occurrence of recorded data.

4.5.2 Interpretation

There are three faults that have been chosen to be used for the understanding of the stress field distribution of the Study area. These faults are thrust and a listric fault which are interpreted from the internal part and towards the north-western part of the Study area. The fault points have been extracted from Petrel[®] 2014 as x, y and z coordinates to estimate the dip azimuth.

The interpreted faults represent the combination of listric and thrust faults. Even though listric faults barely show on our seismic data they were however interpreted to show the general trend at which the faults are striking. Fault 1 mapped listric faults and faults 2 and 3 are thrust faults (which are prevalent in this area of study). The three faults chosen indicate the paleo-stress conditions that are responsible for the brittle deformation events under consideration. Fault one, two and three all show a north-westward trend.

Relating fault trend and fault morphology to the tectonic event interpreted for the Study area will indicate whether the fault planes are contemporaneous with the tectonic evolution of the basin: whether the faults are gravity induced or resulted from a superimposed event reflecting different stress environments and tectonic regimes. The analysed data from rose diagram show a northwest-southeast mean resultant strike. The development of deformation from south to north will also be explained by looking at the stereo-net plots.

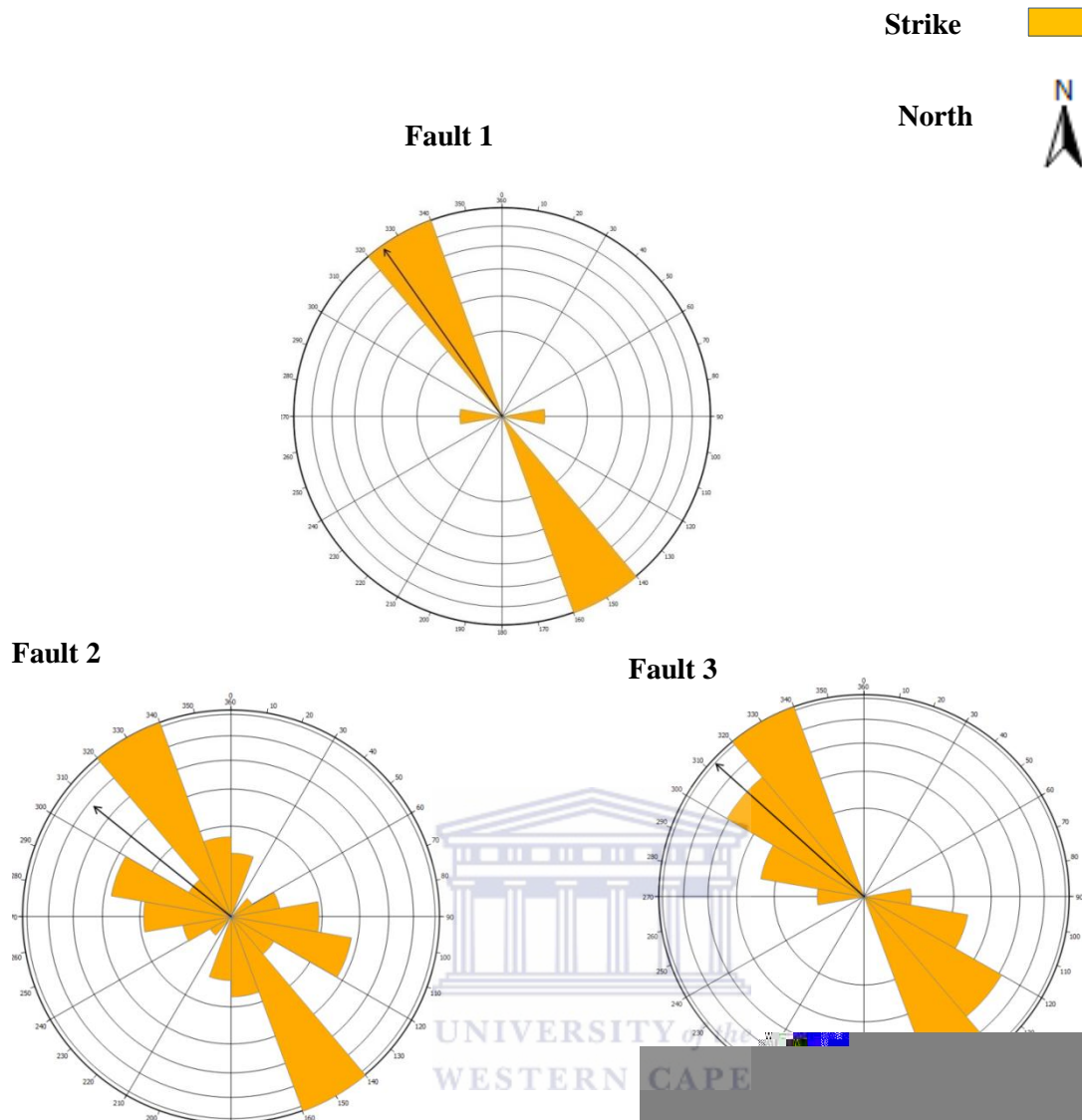


Figure 14: Rose diagrams showing the frequency distribution of dip and strike of faults.

The azimuthal bins are in 30 degree increment and the tally (shading within the azimuthal bins) is the number of fault strikes that occur in each bin. So the rose diagram coupled with stereo-net plot (pi-diagram) will be used to understand the deformational regime responsible for the structures observed in the Study area.

4.6 Stereo-Net Plots Interpretation

4.6.1 Interpretation

An imaginary line perpendicular to the plane is called a pole to the plane. Poles of faults are plotted from the great circles (from beta diagram) and can simply be defined as the poles to planes. Interpreting large numbers of poles to faults is much more accurate and easy to use for kinematic fault analysis than plotting great circles as it is easier and more

accurate to interpret a large number of dots than a large number of overlapping lines. The faults plotted in the rose diagrams (fig.14), confirm the orientation of the faults deduced from the pi-diagrams (fig.15).

Using the thrust faults, the Study area shows that the shortening intensifies to the north where faults are concentrated and this is clearly shown in poles of faults in Figure 15 below.

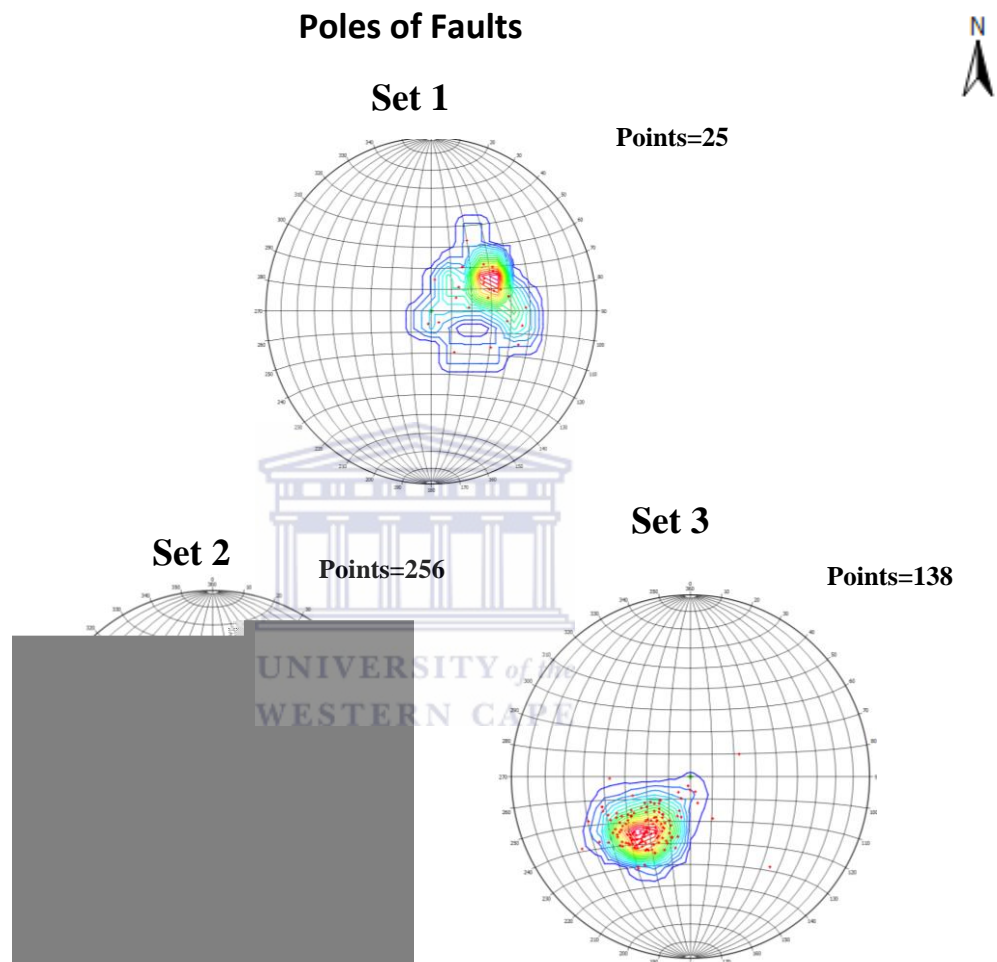


Figure 15: The stereographic projection of faults points. Sets 1 illustrate normal faulting while sets 2 and 3 represent thrust faulting.

Using 2D Move™ to get the poles of faults the fault points were plotted in a stereo-net diagram. Stereographic projections are divided based on the sense of slip (reverse or normal in this study) of the faults.

The faults which have been selected in this interpretation are both thrust and listric faults. The listric fault in this basin dips in the westerly direction and is generally situated in shallower waters than the thrust faults which are dipping in easterly direction.

Using Anderson's theory where he stated that if sigma 1 is vertical then it is an extensional regime, if sigma 3 is vertical then it is a compressional regime and finally if sigma 2 is vertical then the dominant regime is the strike-slip deformation.

Anderson's Fault Classification

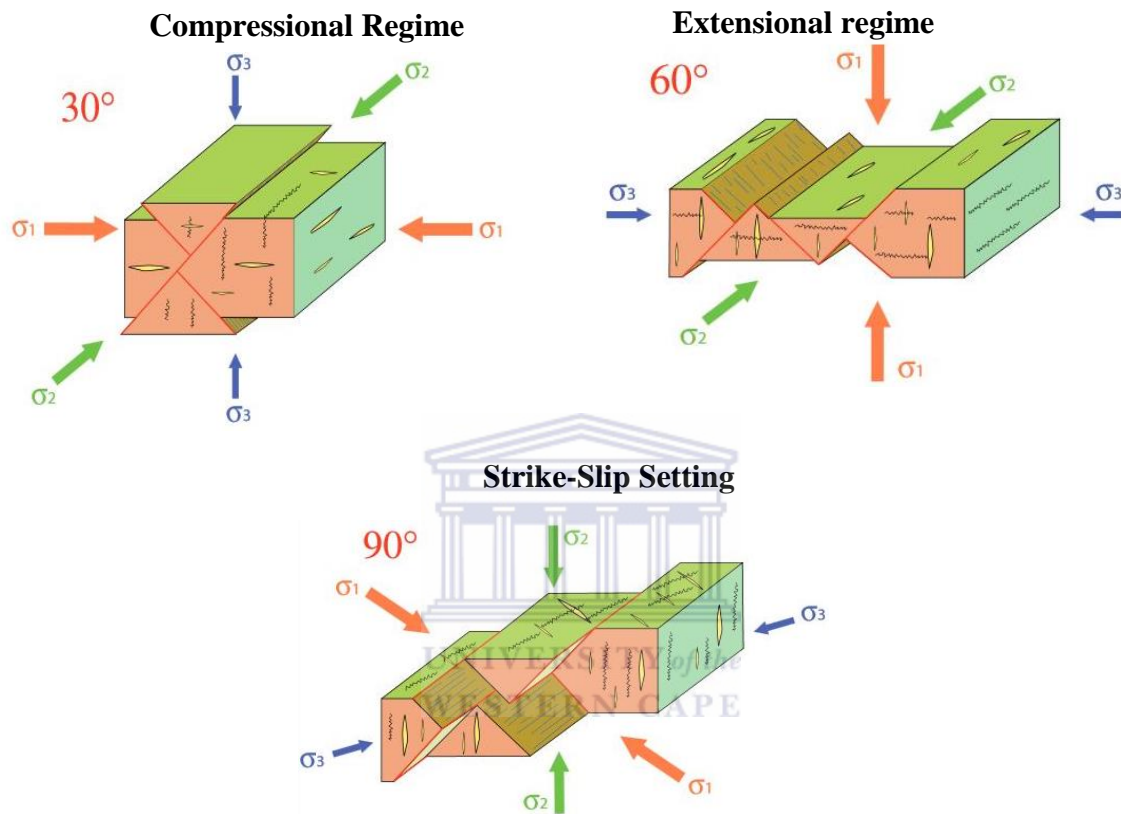


Figure 16: Anderson's fault classification (Yin, 1989).

Thus based on Anderson's theory sigma 1 is vertical in the near shore environment and horizontal on the basin toe or basin end of the section. The focus is on thrust faults because they are the most dominant faults in the Study area and so they hold the key in understanding the strain and stress distribution and the origin of gravity induced deformational features.

CHAPTER 5

5. Discussion

Jungslager *et al.* (1999) suggested that the tectonic processes in the north of the basin initiated rifting which was later followed by flexure subsidence of the shelf and slope which were gravity controlled. Hence, deltaic failure caused by margin uplift was greater in the north as compared to the southern side of the Study area.

The gravity and toe-thrust faulting are bounded at the top and base by two strong reflectors referred to as horizon 1 and 4 respectively (see fig.7 and 11). The isochron map for seismic facies 1, 2 and 3 shows that apparent thickness variation is influenced by the number of thrust faults which increases towards the north of the Study area. The internal seismic section of the southern part of the study generally has no deformational features. Small deformational features along the depositional margin and in the distal southern regions of the Study area have been observed in the seismic data by authors like Kuhlmann, *et al.* (2010) and de Vera *et al.* (2010).

The Study area shows an increase in number of deformational features from northeast to southwest with structures like slump structures, compressional toe-thrusts and horses. To understand the development of deformation in the Study area the following will be discussed:

- 1) The development of deformation using thickness maps and cross sections
- 2) The stress and strain distribution in the Orange Basin
- 3) The origins of the gravity collapse systems of the Orange Basin

5.1 Development in deformation in the Study area

The results from the interpreted seismic sections that are used to clarify the implication of the prominent seismic horizons and major faults are presented in chapter four. Despite a significant amount of research in this area there is still confusion on the relationships between gravity-induced structures, the thickness change and development of deformation in the Study area.

Thickness maps of the horizon 1-2, 2-3 and 3-4 in Figures 8, 9 and 10 respectively reveal thinner sediment packages landward of the Study area. This thickness difference is the

result of the removal of sediments during erosion from the landward side of the basin and redeposition deeper in the basin (Jungslager, 1999). The thickness maps which have been extracted pertaining to the Study area show an increase in apparent thickness towards the north where there is a large number of thrust faults or horse structures. This thicker seismic facies resulted from basinward orientation of faults depicting deep underlying grabens and horst structures that trend sub-parallel to the west coast of South Africa (Paton *et al.*, 2008). The disappearance of seismic horizon 3 may have been the result of erosion further towards the north (fig.7).

Southern areas are partially preserved due to significant slow sedimentation rates and slope processes. The isochore maps show that the main depocentre (indicated by thickening seismic facies) is located in the north western part of the Study area. Steepening and thickening of seismic facies suggests either an increase in sedimentary supply or a stacking of sedimentary layers due to the development of gravity induced faults. Deeper waters created turbidites, channels and associated channel-levee systems due to rapid slope processes and high sedimentation rates which might have resulted in the geometric architecture of the Orange Basin (Kuhlmann *et al.*, 2010).

According to Kuhlmann *et al.*, (2010) the tectonic stress which initiated the opening of the Atlantic Ocean during Gondwana break-up started in the northern side of the area of study and moved towards the south. This opening or extension of the basin was followed by margin uplift which created a north-westwards stress field causing gravitational potential energy contrasts which contributed to the development of the observed faulting system.

5.2 The stress and strain distribution in the Orange Basin

Butler and Paton (2010) and de Vera *et al.* (2010) discovered that there is a mismatch between the minimum estimate of extension (44 km) and slip on thrusts (18–25 km). This mismatch or lack of balance was discovered during structural restorations of the main gravity-driven system between down-dip shortening and up-dip extension. A longitudinal strain component of 18–25 percent is required to compensate for the lack of balance distributed across the system, most reasonably as the result of lateral compaction and volume loss (Butler and Paton, 2010).

According to Granado *et al.* (2009) lack of balance between structural shortening (16 km) and extension (44 km) can be explained by layer parallel shortening accompanied by volume loss in the thrust belt, and inconsistencies between the acquisition of seismic data,

the direction of tectonic movement and location of the seismic line. Widely distributed ductile deformation and substantial amount of the slip required to balance the extensional displacements higher on the slope with compressional displacements on the bottom of the slope must be accommodated by probably volume loss and lateral compaction. This lateral compaction and volume loss presumably predated the localization of thrusts (Butler and Paton, 2010). This is because significant amount of extension has to occur first before any compression can be detected from the seismic data. Lateral strain component external to the deformational system is required to contribute (if not initiated) to the lateral translation during extension. So the deformational features in this study which were proposed to be purely caused by geological processes may have not been the only factor that contributed to the origins of the gravitational tectonics of the Orange Basin.

5.3 The Origins of the gravity collapse systems of the Orange Basin

Even though the controlling factors influencing the gravity collapse structures are poorly understood, the examination of development of deformation from north to south in the Study area shows that gravity collapse structures are controlled by many factors. Understanding the origins of the gravity collapse systems requires the deep understanding of the following:

- 1) Passive margin uplift and thermal subsidence
- 2) Meteorite impact in the Orange Basin
- 3) Slump sediment deformation

5.3.1 Passive margin uplift and thermal subsidence

The models by McKenzie (1978) and Wernicke *et al.* (1985) are widely known and successful models that explain the subsidence and uplift history in the passive margin settings and also in the continental interior. Wernicke (1985) promulgated a simple shear model which predicts the high degree in subsidence and uplift history on either side of the continental basin based on the spatial variation in the mantle thinning and in the changes in the proportions of crust.

The McKenzie model assumes that there is a high degree of symmetry on either side of the rift zone. There are basically three stages for the McKenzie model; (1) Pre-rift phase is the part of the lithosphere which has not been deformed, (2) The stretching phase also known as syn-rift is where continental thinning occurs as the result of the upwelling hot

mantle. A lot of horst and graben and subsidence can be observed in this stage. (3) The cooling or post-rift phase is where stretching ceases and cooling starts to achieve thermal equilibrium. The cooling process thickens the oceanic or continental lithosphere which causes further subsidence.

Since the study focuses on the post-tectonic dynamics events which contributed to its evolutions through its history, the third stage is more appropriate for this study as it outlines the characteristics which are to be expected during a post-rift phase. Thermal subsidence in the Orange Basin was reported by Jungslager (1999). The thermal subsidence is usually followed by mechanical passive margin uplift and this has not only been observed in the Orange Basin but has also been studied and identified among many areas like South China (Lin *et al.* 2003) and Western Mediterranean (Watts *et al.*, 1993).

The Orange Basin represents a typical passive margin evolution with syn-rift and post-rift megasequences. Inadequately imaged transitional zone allows for a down-dip link between extensional and contractional domains. This transitional zone consists of ductile material which absorbed extensional displacement and significant amount of stress external to the deformational system was required to push the transitional zone to initiate thrust faulting. Syn-rift deposition in the Orange Basin is mentioned to have been controlled by extensional faults which occurred as the result of crustal extension and associated mechanical subsidence during the Late Jurassic to Early Cretaceous (160-130 Ma) (Granado *et al.*, 2009). The seaward dipping reflectors (SDRs) in the Orange Basin demonstrate the interaction between crustal extension and thermal subsidence (Séranne and Anka, 2005). Similar to the subsidence of oceanic lithosphere, the post-rift subsidence of extensional basins is mainly governed by thermal relaxation and contraction of the lithosphere, resulting in a gradual increase of its flexural strength, and by its isostatic response to sedimentary loading.

According to Bauer *et al.* (2000) and Granado *et al.* (2009) the syn-rift and post rift megasequences of the Orange Basin were deposited as cooling of the asthenosphere and the underplated igneous material occurred which caused thermal subsidence. This thermal subsidence was succeeded by basin margin cratonic uplift (Gallagher and Brown, 1999) during the Post-rift stage in the early to mid-Cretaceous. Granado *et al.* (2009) developed a tectonostratigraphic model of the basin which showed that a combination of cratonic uplift and thermal subsidence caused gravity collapse tectonics. Thus gravity tectonics of the Orange Basin according Gallagher and Brown (1999) and Granado *et al.* (2009) were

caused by the south-west African passive margin uplift combined with underplating of igneous material which caused thermal subsidence (Bauer *et al.*, 2000).

5.3.2. Meteorite impact in the Orange Basin

It has been shown that all planetary bodies with a solid surface have meteorite impact craters. Based on the morphology, the impact craters are divided into two main groups' i.e. (1) simple crater and (2) complex crater. The characteristics for the simple impact crater include hemispherical or bowl-shaped depression (fig. 17). The impact craters with down-faulted annular troughs and uplifted central area are called complex (Osinski, 2005). The general process in both of the impact crater is that they form as the result of gravitational changes during the modification stage of impact crater formation. Most studies on impact craters have been focused on the terrestrial terranes because that is where most impact craters have been discovered. There is limited literature on the main characteristics of the marine impact craters.

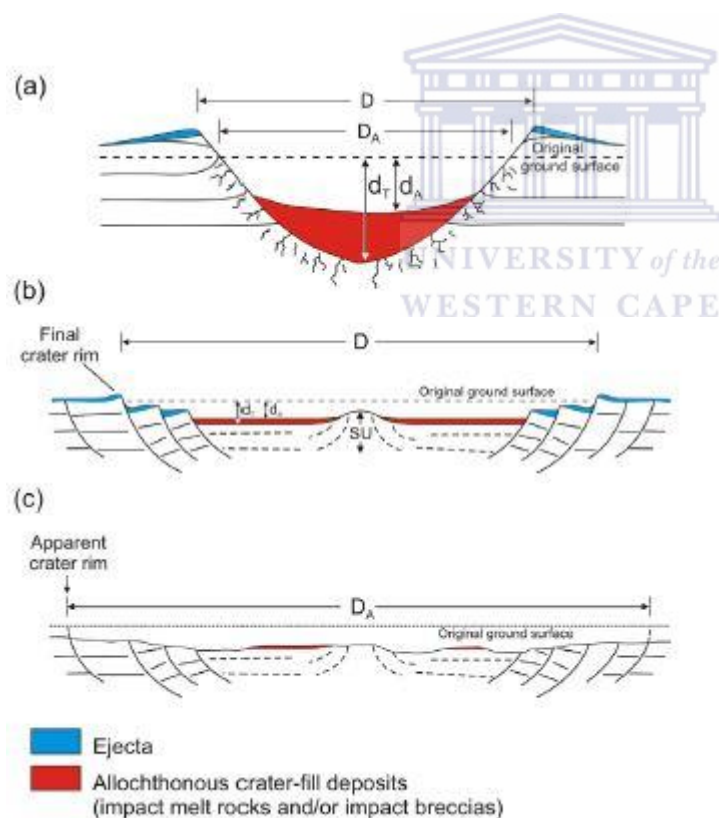


Figure 17: Schematic representation of the simple (a) and complex impact crater (b, c) formations. (After Osinski, 2005)

Wall (2008) noted that the presence of a water column for marine impact craters affects all stages of the meteorite impact which then creates geomorphological features which are different than the terrestrial impact craters. According to Osinski (2005) the kinetic

energy of the impact crater transfers shock waves which spread-out as rarefaction or tensional waves which creates compression and subsequent instantaneous melting and/or vaporization of a volume of target material close to the point of impact as the result of the high strain component by the impact.

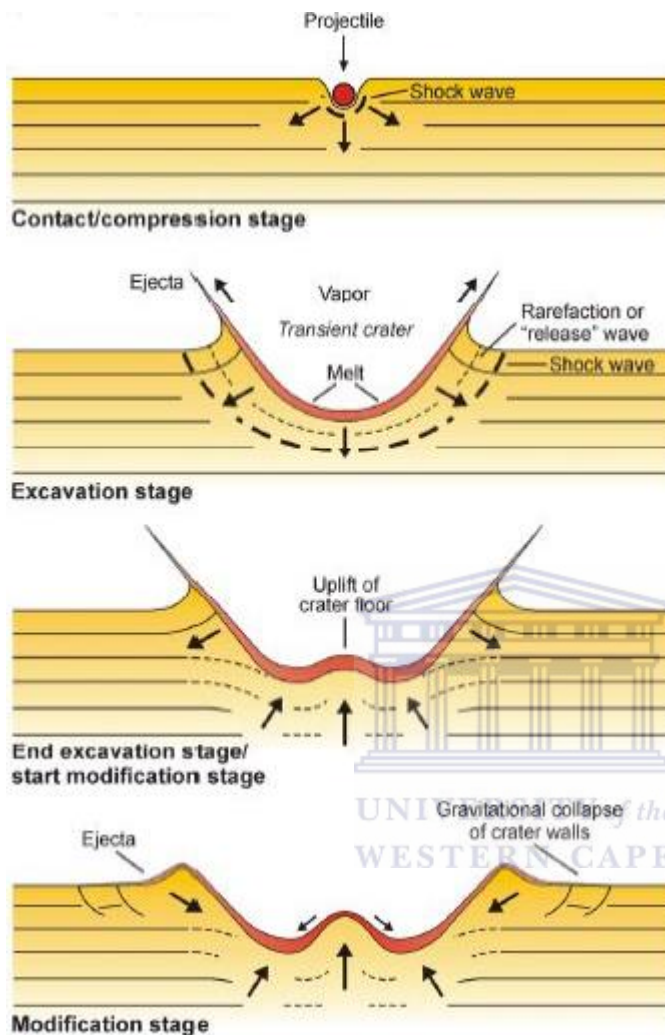


Figure 18: Stages for the formation of the meteorite impact. (After Osinski, 2005)

Geophysical evidence has been used to investigate the impact craters because over the years in has been discovered that geophysical evidence or measurements have played a major role in differentiating depressions which form as the result of volcanoes, salt diapirs and glaciogenic effects (Mhlambi, 2014). Seismic reflection profiles have been used to identify impact craters by looking for typical characteristics like concentric or radial fault distribution, central uplifts and concentric rings of folds and these features are very distinct in the seismic data (Glikson and Uysal,2013; Mhlambi, 2014).

Significant evidence to suggest that the far-field impact of the meteorite impact influenced gravity and toe-thrusting faults is outlined below with reference to the recent work by Mhlambi (2014). Even though seismic interpretation does not provide unequivocal evidence for the impact crater it is however a good start to explain buried structures for offshore environment given the limitation of data in this study.

The thesis presented by Mhlambi (2014) investigated the geometry, morphology, extent and age of the crater-like feature found buried at approximately 280 metres below sea floor in the Orange Basin. The circular crater is buried within Cretaceous and Cenozoic age marine sediments. The work by de Vera *et al.* (2010) suggested that the age of the gravity collapse structures for this Study area spanned from the Coniacian to the Santonian Epochs. While on the other hand Jungslager (1999) and Paton *et al.*, (2008) suggested that gravity collapse systems occurred between the Cenomanian to Maastrichtian Epochs. These deformational periods are within the Cretaceous and early Cenozoic age marine sediments which is the time where a possible meteorite might have impacted the Orange Basin.

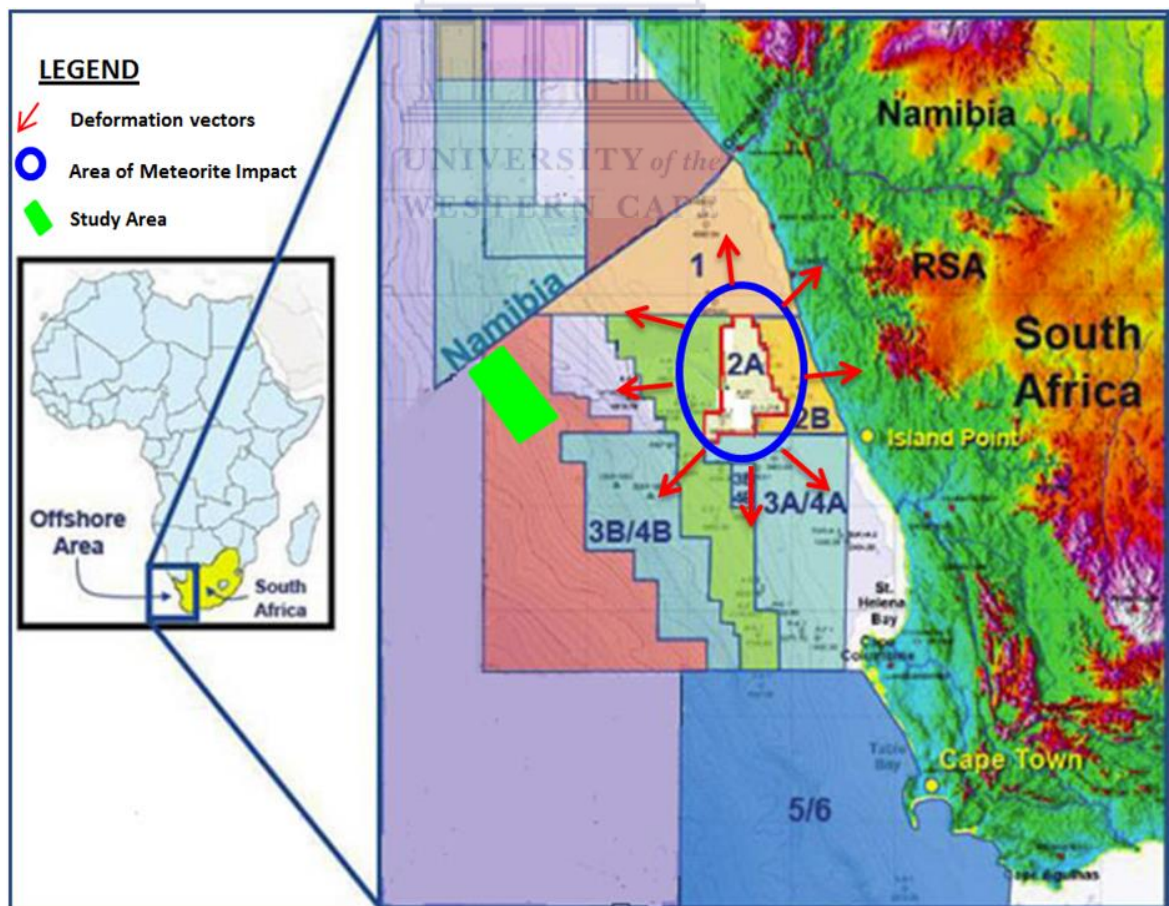


Figure 19: Outward propagation of deformation vectors as the result of a probable bolide impact. Adapted from www.upstreamonline.com and modified after Mhlambi (2014).

Figure 19 above illustrates an exploration area where a probable impact crater was discovered. The deformation vectors might have created gravitational energy contrast which formed concentric folds (fig.20 below). The Study area comprises exploration licence Block 2A, which lies approximately 380 kilometres northwest of Cape Town in the northern part of the Orange Basin.

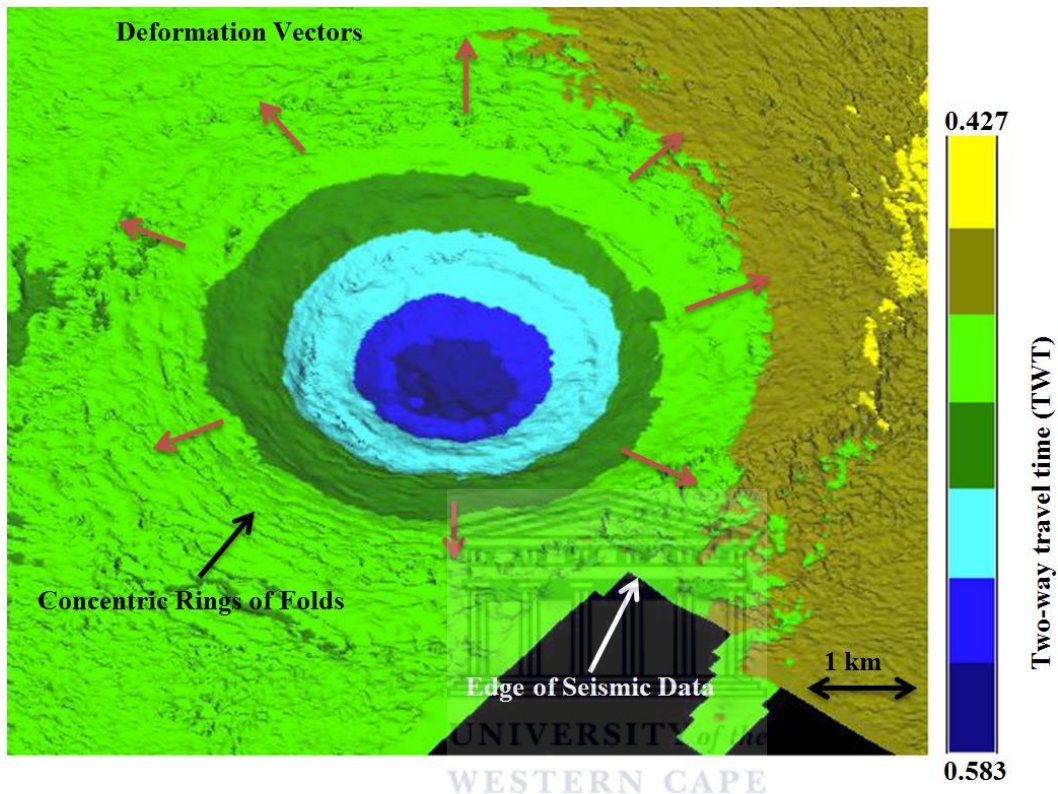


Figure 20: Three-dimensional view of the structure mapped at the base of the Cenozoic strata, adapted and modified from Mhlambi (2014).

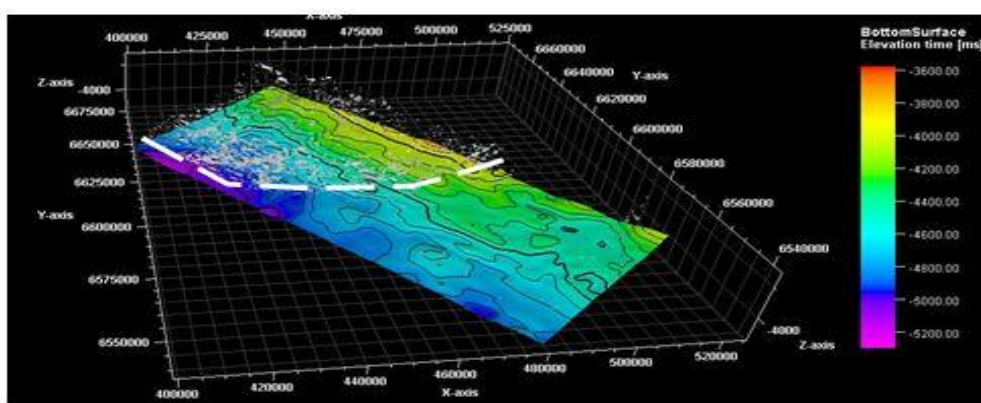


Figure 21: Automatic fault extraction from Petrel® 2014 using 3-D seismic data for this study shows a concentric distribution of faults.

Distribution of these faults shows a hemispherical structure and this is likely the result of the far-field effect of the meteorite impact which is shown in Figure 20. The morphology

of the crater (fig.17) resembles that of meteorite impact craters which can be classified as a probable impact crater (Mhlambi, 2014). Figure 20 shows concentric distribution of faults as the result of outward distribution of deformation vectors. The possible meteorite impact (fig.17) then created series of concentric folds extending outward from the central crater. This crater hypothesis by Mhlambi (2014) was proposed instead of the coalescing gas chimneys that define a circular shape which is promulgated by Hartwig *et al.* (2012). This is because the gas-chimneys do not form perfectly circular geological depressions and the diametres of gas chimneys are typically smaller compared to that of a bolide impact crater.

5.3.3 Slump sediment deformation

Huge slope failures have been documented in many parts of the world including the passive continental margins. The presence of the superimposed tectonic structures makes it difficult to recognize slump-sediment deformation. Recognizing the overall kinematic style and the physical state of the structures is very difficult especially where there are superimposed tectonic structures. Addressing the typical characteristics of the slump deformation one should look at the questions required to address the overall kinematic style, the sediment flow rate (high or low), physical state (lithified or unlithified) and the difference in competencies (degree any which the rock resist to deform or erode).

The following section describes the typical slump-sediment deformation features which will be compared to the observed structural features of the seismic data. Deformation structures that formed between horizon one and horizon four are described; this is done with the focus on describing the difference in competencies between the sedimentary layers which has been caused by slump-sediment deformation. The focus here is not dating the deformation, or restoring the deformed structures, the focus here is to logically explain how the geometric architecture of Orange Basin came to be as the result of slump-sediment deformation.

The understanding of slump sediment deformation looks at the reasons why the sediments above the green line are not thrustured but the sediments below are thrustured (fig.22 below). The explanation will be the difference in competency of the sediments at the time the slope reached the critical angle of repose.

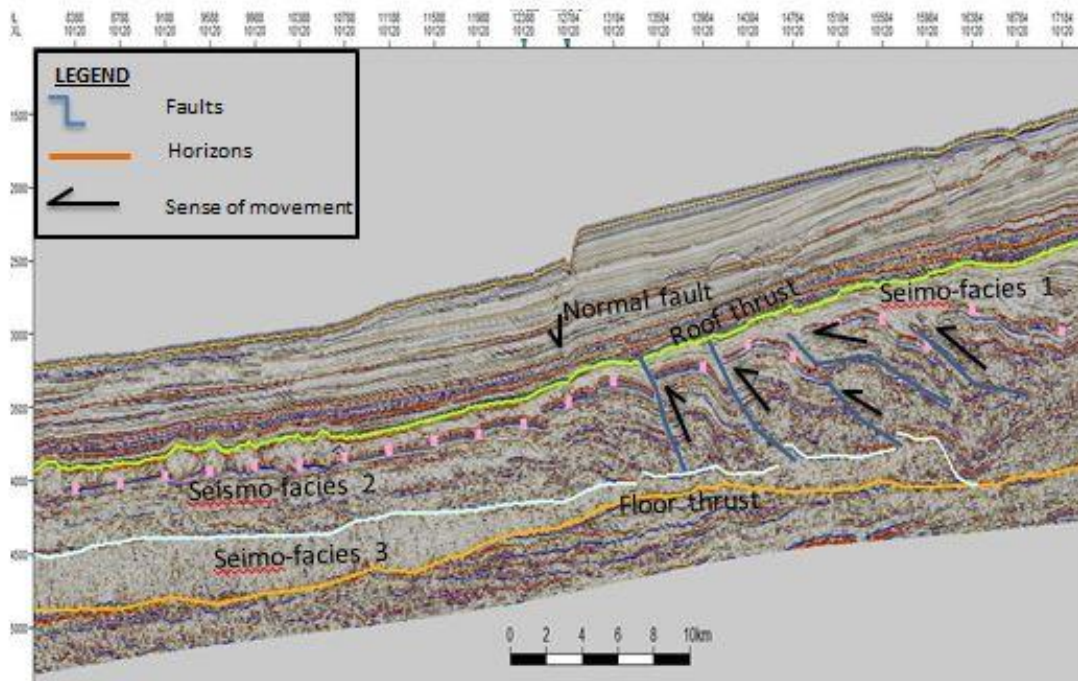


Figure 22: The Figure above shows the interpreted seismic horizons which have been used to understand the geomorphological and structural geometry of the Study area. Seimo-facies 1, 2 and 3 are also depicted.

Below the white line (fig.22) sediments were too consolidated and had a different angle of repose than the middle package (seimo-facies 1 and 2) which produced horse structures. The greyish white layer which is below the green horizon (seismo-facies 1) could have been an unconsolidated top layer during thrusting or it was a later deposit filling up the gaps formed by the sub-sediment slumping. This greyish white layer produced a new flat surface where the top relatively undeformed package was deposited on top of it (above the roof thrust).



Figure 23: Duplex structure in dolomitic sandstones near Svalbard. Note the horses, floor thrust and roof thrust (after Fossen. 2010).

Figure 23 shows a real-life example of a roof, floor thrusts and horse structures which have been depicted throughout the Study area. Note stacking sequence of thrust faults forming horse structures similar to the ones observed in Figure 22 above. The normal fault (fig.22) down-throws the top package towards the left side of the slope. This normal fault does not penetrate to the thrust area and this could be an indication of difference in competencies of the deposited layers. The difference in competencies can also indicate a hiatus or time gap between the layers above and below the green horizon.

Interpretation of the mechanisms

1. High sedimentation rates associated with rapid delta progradation caused aggradational stacking along a steep depositional margin resulted in the distal regions of the Orange Basin to be relatively unstable. This caused the development of extensional growth faults, large slump structures and associated compressional toe thrusts or horse structures.
2. Then tilting and a layer parallel stress field developed. This layer parallel stress field was too weak to affect the relatively competent top part but it was strong enough to affect the incompetent middle package (ductile material in the transitional zone) resulting in roof thrust and sole thrust. The roof and floor thrust which formed, constrained the thrust faults or horse structures as the result of the competency difference between the layers above and below the green horizon.
3. There was a high impact crater which as the result of far-field effect, created concentric folds and a hemi-spherical faults distribution, which may have contributed to the movements of thrust faults as seen in seismic section. This impact crater possibly resulted in margin uplift, extensional displacements, ductile deformation and volume loss.
4. The extensive ductile material, lateral compaction and penetrative layer-parallel shortening in poorly lithified rocks could lead to substantial heterogeneity in the permeability and porosity characteristics of the reservoirs; this could have a negative effect on hydrocarbon production.

CHAPTER 6

6.1 Conclusion

The gravity induced faults are late tectonic and they are a reflection of geological events which occurred to influence the movement of post dynamic geometry. The four interpreted horizons (1, 2, 3 and 4) show a strong change in seismic patterns, continuity and amplitude from the south, via the centre to the north. A combination of tectonic events resulted in a significant change in the deformation style in the post-rift evolution. These events include the combined effects of thermal subsidence, margin uplift and bolide impact.

The lack of balance during structural restoration coupled with an unknown strain component, possible volume loss and the observed concentric distribution of faults to the North of the Study area, support the probable bolide impact hypothesis. So the combined effect of stress field and thrust faulting on the observed thickness change in seismic facies 2 is not enough to explain the gravity collapse structures. It is therefore concluded that gravity collapse systems of the Orange basin was caused by a combinations of geological processes like margin uplift, delta progradation and tectonic subsidence (which caused slump sediment deformation) and also a probable meteorite impact.

6.2 Recommendation

We should look at the origins of the gravity induced collapse structures using seismic data with well data to perform depth conversion and to ascertain the depositional period for the interpreted horizons in this study. Understanding gravitational systems lies in the kinematic evolution of the basin's deformational domains. Local and regional stress field distribution studies are required to understand the geodynamic evolution and the lack of structural balance in the basin. The detailed studies for compressional and extensional systems have to be tested against the deformation requirements for the whole gravitational system in its regional context. 3-D Geological modelling with computerized simulation of the possible formation or origins of the gravity collapse of the Study area is required.

REFERENCES

- Alsop G.I., Marco, S., 2013. Seismogenic slump folds formed by gravity-driven tectonics down a negligible subaqueous slope. *Tectonophysics*, 605, 48–69.
- Angelier, J., 1994. Fault slips analysis and paleostress reconstruction. In: *Continental deformation* (edited by Hancock P.L.). Pergamon Press Ltd, Oxford, 53-100.
- Baroň, I., Kernstocková, M., Faridi, M., Bubík, M., Milovský, R., Melichar, R., Sabouri, J., Babůrek, J., 2013. Paleostress analysis of a gigantic gravitational mass movement in active tectonic setting: The Qoshadagh slope failure, Ahar, NW Iran. *Tectonophysics*, 605, 70–87.
- Bauer, K., Neben, S., Schreckenberger, B., Emmermann, R., Hinz, K., Fechner, N., Gohl, K., Schulze, A., Trumbull, R.B., Weber, K., 2000. Deep structure of the Namibia continental margin as derived from integrated geophysical studies. *Journal of Geophysical Research* 105, 25829.
- Brown, L.F. Jr., Benson, J.M., Brink, G.J., Doherty, S., Jollands, A., Jungslager, E.H.A., Keenan, J.H.G., Muntingh, A., van Wyk, N.J.S., 1995. *Sequence Stratigraphy in Offshore South African Divergent Basins. An Atlas on Exploration for Cretaceous Lowstand Traps* by Soekor (Pty) Ltd. AAPG studies in Geology # 41, iii-vii.
- Butler, R.W.H., Paton, D.A., 2010. Evaluating lateral compaction in deepwater fold and thrust belts: How much are we missing from “nature’s sandbox”? *Geological Society of America Today*, vol. 20 (3): 1-7.
- Cameron, M., Fomel, S., Sethian, J., 2008. Time-to-depth conversion and seismic velocity estimation using time-migration velocity. *Geophysics*, vol. 73, 205-210.
- Célérier B., 1988. How much does slip on a reactivated fault plane constrain the stress tensor?. *Tectonics*, 7, 1257-1278.

- Chigira, M., Hariyama, T. and Yamasaki, S., 2013. Development of deep-seated gravitational slope deformation on a shale dip-slope: Observations from high-quality drill cores. *Tectonophysics*, 625, 104-113.
- Cloetingh, S., Kooi, H., 1988. Intraplate stresses and dynamic aspects of rifted basins. *Tectonophysics*, 215, 167-185.
- Crosta, G.B., Frattini, P., Agliardi, F., 2013. Deep seated gravitational slope deformations in the European Alps. *Tectonophysics*, 605, 13-33.
- de Vera J.D., Granado, P., McClay, K., 2010. Structural evolution of the Orange Basin gravity driven system, offshore Namibia. *Marine and Petroleum Geology*, 27, 223-237.
- Ezekiel J.C., Onu, N.N., Akaolisa, C.Z., Opara, A.L., 2013. Preliminary interpretation of gravity mapping over the Njaba sub-basin of southeastern Nigeria: An implication to petroleum potential. *Journal of Geology and Mining Research*, 5 (3), 75-87.
- Fossen, H., 2010. *Structural Geology*. Cambridge, United Kingdom, Cambridge University press, 313-315.
- Gallagher, K., Brown, R., 1999. Denudation and uplift at passive margins: the record on the Atlantic Margin of southern Africa. *The Royal Society Journal* 357, 835-859.
- Gerrard, I., Smith, G.C., 1982. Post-Paleozoic Succession and Structure of the Southwestern African Continental Margin. *Stud. Cont. margin Geol. AAPG Memoir* 34 (1), 49-74.
- Glikson, A., and Uysal, I.T., 2013, 'Geophysical and structural criteria for the identification of buried impact structures, with reference to Australia', *Earth-Science Reviews*, 125, 114-122.
- Granado, P., de Vera, J., McClay, K.R., 2009. Tectonostratigraphic Evolution of the Orange Basin, South-West Africa. *Yorsget Meeting Extended Abstract*, July 2008, Oviedo (Spain). *Department of Geology, University of Oviedo*, 29: 321-328

- Hersthammer, J. & Fossen, H., 1999. Evolution and geometries of gravitational collapse structures with examples from the Statfjord Field, northern North Sea. *Marine and Petroleum Geology*, 16, 259-281.
- Hirsch, K.K., Scheck-Wenderoth, M., van Wees, J.-D., Kuhlmann, G. & Paton, D.A., 2010. Tectonic subsidence history and thermal evolution of the Orange Basin. *Marine and Petroleum Geology*, 27, 565–584.
- Jaboyedoff, M., Penna, I., Pedrazzini, A., Baron, I. & Crosta, G.B., 2013. An introductory review on gravitational-deformation induced structures, fabrics and modelling. *Tectonophysics*, 605, 1-12.
- Jungslager, E.H.A., 1999. Petroleum habitats of the Atlantic margin of South Africa. *Geological Society of London, Special Publication*, 153, 153–168.
- Khani,H.F., 2013. Three-dimensional analysis of syndepositional faulting and synkinematic sedimentation, Niger Delta, Nigeria, 18-45.
- Kramer E.A.J., Heck L., 2013. Orange Basin 3D™ pre-processing and PreSDM. Shell Global Solutions international B.V., Rijswijk, 1-7.
- Kuhlmann, G., Adams, S., Anka, Z., Campher, C., di Primio, R. & Horsfield, B., 2010. 3D petroleum system modellin within a passive margin setting, Orange Basin, block 3/4, offshore south Africa - Implications for gas generation migration and leakage. *South African Journal of Geology*, 114, 387–414.
- Leyshon, P., R. Lyle., 2004. *Stereographic Projection Techniques in Structural Geology*. Cambridge: Cambridge University Press. Page: 1-43.
- Lin, A.-T.,Watts, A.D and Hesselbo. S.P., 2003. Cenozoic stratigraphy and subsidence history of the South China Sea margin in the Taiwan region, *Basin Research*, 15, 453-478.
- Maloney,D., Davies R., Imber, J., King,S., 2012. Structure of the footwall of a listric fault system revealed by 3D seismic data from the Niger Delta. *Basin Research*, 24, 107-123.

- McKenzie, D., 1978. Some remarks on the development of sedimentary basins. *Earth and Planetary science letters*, Amsterdam, 40, 25-32.
- McMillan, I.K., 2003. Foraminiferally defined biostratigraphic episodes and sedimentation pattern of the Cretaceous drift succession (Early Barremian to Late Maastrichtian) in seven basins on the South African and southern Namibian continental margin. *South African Journal of Science*, 99, 537–576.
- Mhlambi, S., 2014. The possible meteorite impact on the Orange Basin. Unpublished Honor=s thesis. Cape Town: University of Cape Town. Page: 18-29.
- Muntingh, A., 1993. Geology, prospects in Orange Basin offshore western South Africa. *Oil and Gas Journal*, 106–109.
- Muntingh, A., Brown L. F., J., 1993. Sequence Stratigraphy of Petroleum Plays, Post-Rift Cretaceous Rocks (Lower Aptian to Upper Maastrichtian), Orange Basin, Western Offshore, South Africa, in: Weimar, P., Posamentier, H. (Eds.), *Siliciclastic Sequence Stratigraphy, Recent Developments and Applications*; AAPG Memoir 58. The American Association of Petroleum Geologists, Tulsa, Oklahoma, U.S.A, 71–98.
- Osinski, G.R., Spray, J.G., Lee, P., 2005. Impactites of the Haughton impact structure, Devon Island, Canadian High Arctic, *Meteoritics & Planetary Science*, 40, 1789–1812.
- Pandey, A.K., Kumar, R., Shukla, M., Negil, A., Tandon, A.K., 2013. Seismic velocity model building: an aid for better understanding of subsurface a case study from Cambay basin, India. 10th Biennial International Conference and Exposition, P408.
- Paton, D.A., van der Spuy, D., di Primio, R., Horsfield, B., 2008. Tectonically induced adjustment of passive-margin accommodation space; influence on the hydrocarbon potential of the Orange Basin, South Africa. *AAPG Bulletin*, 92, 589–609.
- Rowan, M.G., Peel, F.J., and Vendeville, B.C., 2004, Gravity-driven fold belt on the passive margins, *AAPG Memoir* 82:157-182

- Salomon, E., Koehn, D., Passchier, C., Hackspacher, P.C. & Glasmacher, U. A., 2014. Contrasting stress fields on correlating margins of the South Atlantic. *Gondwana research*, 01326, 1-16.
- Séranne, M., Anka, Z., 2005. South Atlantic continental margins of Africa: A comparison of the tectonic vs climate interplay on the evolution of equatorial West Africa and SW Africa margins. *Journal of African Earth Science*, 43, 283–300.
- Tavani, S., Storti, F., Lacombe, O., Corradetti, A., Muñoz, J.A., Mazzoli, S., 2014. A review of deformation pattern templates in foreland basin systems and fold-and- thrust belts: Implications for the state of stress in the frontal regions of thrust wedges *Earth Science reviews*, 141, 82-104.
- Wall, M.L.T., 2008, '3D Seismic Analysis of the Silverpit Structure', PhD Thesis, Cardiff University. Page: 1 of 21- 1of 43.
- Walsh, J.P., Nittrouer, C.A., 2003. Contrasting styles of off-shelf sediment accumulation in New Guinea. *Marine Geology*, 196, 105-125. Watts, A.B., Platt, J.P., Buhl, P., 1993. Tectonic evolution of the Alboran Sea Basin. *Basin Res.*, 5,
- Watts, A.B., Platt, J.P., Buhl, P., 1993. Tectonic evolution of the Alboran Sea Basin. *Basin Res.* 5, 153-177.
- Wernicke, B., Walker, J.D., Beaufait, M.S., 1985, Structural discordance between Neogene detachment and frontal Sevier thrusts, central Mormon Mountains, Southern Nevada: *Tectonics*, 4, 213-246.
- Yin, a., 1989. Origin of regional, rooted low-angle normal faults: a mechanical model and its tectonic implications. *Tectonics*, vol. 8 (3), 469-482.
- Ziegler, P.A & Cloetingh, S., 2004. Dynamic processes controlling evolution of rifted basins. *Earth Science reviews*, 1-50.